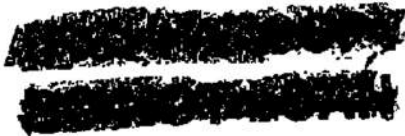


16



NAVORD REPORT

3665

AEDC-TR-54-33

DEC 3 1965
JUL 21 1967

PROPERTY OF U. S. AIR FORCE
AEDC LIBRARY
AF 40(100)-E20

PERFORMANCE OF A CONVERGING-DIVERGING WIND TUNNEL
DIFFUSER IN THE PRESENCE OF A SCAVENGING SCOOP

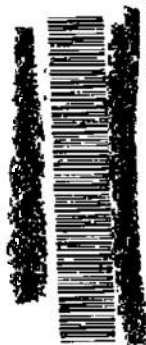
This document has been approved for public release
its distribution is unlimited. *Per TRP 74-21,
dated 11 Oct, 1974*

1 APRIL 1954



PROPERTY OF U. S. AIR FORCE
AEDC LIBRARY
AF 40(100)1200

U. S. NAVAL ORDNANCE LABORATORY
WHITE OAK, MARYLAND



UNCLASSIFIED
NAVORD Report 3665

Aeroballistic Research Report 223

PERFORMANCE OF A CONVERGING-DIVERGING WIND TUNNEL
DIFFUSER IN THE PRESENCE OF A SCAVENGING SCOOP

By:

S. M. Hastings

ABSTRACT: The Naval Ordnance Laboratory, under Air Force contract MIPR R-53-4-AEDC, determined the performance of a variable-area, supersonic wind tunnel diffuser in the presence of a scavenging scoop.

*461
1246
788
1974*

The investigation was conducted at nominal Mach numbers 1.9, 2.5, 2.8, 3.2, 4.3 and 4.9 in the continuous NOL 18 x 18 cm closed-jet Aerophysics Tunnel No. 3. The diffuser consisted of a converging-diverging, two-dimensional, variable area duct. The scavenging scoop, whose inlet was in the same tunnel cross-section as the diffuser inlet, was essentially a hollow cylinder whose axis of symmetry lay along the tunnel centerline. The scoop, which scavenged approximately ten per cent of the impinging flow, terminated in and was supported by a hollow airfoil spanning the tunnel immediately downstream of the adjustable diffuser. The airfoil was connected through the tunnel wall to a suction line through which the scavenged flow was removed. Two diffuser throat locations were investigated.

Operating and starting pressure ratios of the wind tunnel with the scoop removing the impinging flow were determined. The pressure recoveries obtained showed that the longer supersonic diffuser length resulted in the higher recoveries at each Mach number investigated. The highest pressure recovery obtained was 1.09 times the pitot pressure in the test section at $M = 3.24$. Diffuser sidewall static pressure distributions indicated that the larger amount of the static pressure rise was accomplished in the supersonic diffuser.

U. S. NAVAL ORDNANCE LABORATORY
WHITE OAK, MARYLAND

1
UNCLASSIFIED

UNCLASSIFIED
NAVORD Report 3665

The presence of the scavenging scoop lowered the pressure recovery, increased the minimum starting and operating area ratios, and made less favorable the starting pressure ratio. However, the improvement in pressure recovery with convergence as compared to no convergence of the supersonic diffuser ranged from 2 per cent at $M = 1.86$ to 43 per cent at $M = 4.92$, while the starting pressure ratio with convergence as compared to no convergence of the supersonic diffuser improved from 0 per cent at $M = 1.86$ to 24 per cent at $M = 4.92$.

UNCLASSIFIED

NAVORD Report 3665

1 April 1954

The performance of a converging-diverging, supersonic wind tunnel diffuser incorporating a scavenging scoop has been determined. The results are presented in graphical form and as schlieren photographs.

The data were obtained during the last nine months in the 18 x 18 cm Aerophysics Tunnel No. 3. This work was sponsored by the Air Force under task number NOL-226-54.

This document may include technical data or other information which may be proprietary to parties other than the Government, and therefore the transmission by the Department of the Navy of this document is not to be regarded by implication or otherwise as licensing or conveying any rights or permission to the recipient or any other person or corporation gaining access to this document to use for commercial purposes, as distinguished from Governmental purposes, the said technical data or information disclosed herein.

The author wishes to acknowledge the contributions of the Aerophysics and Aeroballistic Operations Divisions. In particular the advice of Dr. R. E. Wilson and Mr. A. H. Lange, the mechanical design work of Messrs. F. Geineder and M. Schlesinger, the assistance in conducting the experimental work by all the members of the Aerophysics Branch II and the many nights of plant operation by Messrs. A. Platnick, W. Brewbaker, G. Baum and A. Riley are acknowledged and greatly appreciated.

EDWARD L. WOODYARD
Captain, USN
Commander

H. H. KURZWEG, Chief
Aeroballistic Research Department
By direction

UNCLASSIFIED
NAVORD Report 3665

CONTENTS

	Page
I. Introduction	1
II. Test Equipment	2
III. Test Procedure	3
IV. Results	5
V. Conclusion	10
VI. References	12

ILLUSTRATIONS

- Figure 1. Duct Configuration, Schematic
- Figure 2. Drawing of the Scavenging-Scoop Models
- Figure 3. Photograph of the West Side of the NOL 18 x 18 cm Aerophysics Tunnel No. 3 with the Long Scavenging-Scoop Model Installed
- Figure 4. Photograph of the West Side of the NOL 18 x 18 cm Aerophysics Tunnel No. 3 with the Short Scavenging-Scoop Model Installed
- Figure 5. Photograph of the East Side of the NOL 18 x 18 cm Aerophysics Tunnel No. 3 Showing the Chamber and Scavenging-Scoop Suction Lines
- Figure 6. Maximum Free Duct Cross-Section Along the Diffuser
- Figure 7. Diffuser Entrance $1/2$ Angle and Subsonic Diffuser $1/2$ Angle as a Function of Diffuser Area Ratio
- Figure 8. Reynolds Number versus Mach Number
- Figure 9. Starting Pressure Ratio versus Diffuser Area Ratio
- Figure 10. Minimum Starting Area Ratio as a Function of Mach Number
- Figure 11. Minimum Operating Area Ratio as a Function of Mach Number
- Figure 12. Pitot Pressure Recovery for $M = 1.86$
- Figure 13. Pitot Pressure Recovery for $M = 2.48$.
- Figure 14. Pitot Pressure Recovery for $M = 2.83$

- Figure 15. Pitot Pressure Recovery for $M = 3.24$
- Figure 16. Pitot Pressure Recovery for $M = 4.30$
- Figure 17. Pitot Pressure Recovery for $M = 4.92$
- Figure 18. Optimum Pitot Pressure Recovery as a Function of Mach Number
- Figure 19. Optimum Supply Pressure Recovery as a Function of Mach Number
- Figure 20. Sidewall Static Pressure Distribution, $M = 1.86$ & $l/H = 2.12$
- Figure 21. Sidewall Static Pressure Distribution, $M = 1.86$ & $l/H = 3.36$
- Figure 22. Sidewall Static Pressure Distribution, $M = 2.48$ & $l/H = 2.12$
- Figure 23. Sidewall Static Pressure Distribution, $M = 2.48$ & $l/H = 3.36$
- Figure 24. Sidewall Static Pressure Distribution, $M = 2.83$ & $l/H = 2.12$
- Figure 25. Sidewall Static Pressure Distribution, $M = 2.83$ & $l/H = 3.36$
- Figure 26. Sidewall Static Pressure Distribution, $M = 3.24$ & $l/H = 2.12$
- Figure 27. Sidewall Static Pressure Distribution, $M = 3.24$ & $l/H = 3.36$
- Figure 28. Sidewall Static Pressure Distribution, $M = 4.30$ & $l/H = 2.12$
- Figure 29. Sidewall Static Pressure Distribution, $M = 4.30$ & $l/H = 3.36$
- Figure 30. Sidewall Static Pressure Distribution, $M = 4.92$ & $l/H = 2.12$
- Figure 31. Sidewall Static Pressure Distribution, $M = 4.92$ & $l/H = 3.36$

- Figure 32. Schlieren Photographs of the Flow
at $M = 1.86$
- Figure 33. Schlieren Photographs of the Flow
at $M = 2.48$
- Figure 34. Schlieren Photographs of the Flow
at $M = 3.24$
- Figure 35. Schlieren Photographs of the Flow
at $M = 4.30$
- Figure 36. Schlieren Photographs of the Flow
at $M = 4.92$
- Figure 37. Schlieren Photographs Showing the
Effect of Diffuser Area Ratio at
 $M = 4.30$ on the Flow in the Super-
sonic Diffuser

LIST OF SYMBOLS

A^*	Nozzle throat area
A^{**}	Diffuser throat area
A_S^{**}	Scoop cross-sectional area at the diffuser throat
A_{SI}	Scoop cross-sectional area at scoop inlet
A_{TS}	Test section area
H	Nozzle exit height = test section height = diffuser entrance height
l	Distance from diffuser entrance to diffuser throat
l_A	Adjustable diffuser length
l_{TS}	Test section length
M	Mach number of test section flow
p	Static pressure (free stream) corresponding to M
P_{wall}	Diffuser sidewall static pressure
P_0	Supply pressure
P_{0E}	End pressure, sphere pressure at flow breakdown
$P_{0E_{opt}}$	Optimum end pressure for a specified Mach number and throat location
P_p	Test section pitot pressure corresponding to M
P_{sphere}	Pressure in the sphere usually given for starting conditions
Re	Reynolds number based on $H = 18$ cm, $T_0 = 15^\circ\text{C}$, and $P_0 = 750$ mm Hg abs.

UNCLASSIFIED
NAVORD Report 3665

T_0	Supply temperature
x	Distance from diffuser inlet to any static tap location
θ	Diffuser entrance half-angle measured from the diffuser centerline
ϕ	Subsonic diffuser half-angle measured from the diffuser centerline
$\frac{A^{**} - A_S^{**}}{A_{TS} - A_{SI}}$	Diffuser area ratio
l/H	Dimensionless supersonic diffuser length
x/H	Dimensionless distance from diffuser entrance to any static tap location
P_{0E}/P_0	Supply pressure recovery
P_{0E}/P_p	Pitot pressure recovery
$P_{sphere}/P_{0E_{opt}}$	End pressure ratio
P_{sphere}/P_0	Starting pressure ratio

II. TEST EQUIPMENT

4. The continuous NOL 18 x 18 cm Aerophysics Tunnel No. 3 and its diffuser mechanism is described in reference (a). A schematic drawing of the tunnel duct configuration is given in Figure 1. The supply air is taken from the atmosphere through a drier into the tunnel and thence into the vacuum sphere. The sphere is normally evacuated by a set of six vacuum pumps or may be evacuated by the centrifugal compressors used primarily for operating the Continuous NOL 40 x 40 cm Aeroballistics Tunnel No. 2. Tunnel inlet conditions are: (1) Supply pressure slightly below atmospheric due to the pressure drop across the drier which is dependent upon Mach number; (2) average supply temperature of 12°C; and (3) dew point of ~ -30°C.

5. The diffuser consists of two pairs of hinged plates forming a convergent-divergent duct between the parallel sidewalls. The diffuser throat is at the hinges and was located 33.750 inches or 4.76 H downstream from the nozzle exit. An electric drive is provided to open and close the diffuser throat. For one configuration the diffuser entrance was located 10 inches or 1.40 H downstream of the nozzle exit and for the other configuration the diffuser entrance was located 18.750 inches or 2.64 H downstream. The corresponding supersonic diffuser lengths (the distance from the diffuser entrance to the throat) were 3.36 H and 2.12 H, respectively. With the diffuser throat at its maximum opening the tunnel cross-section is constant from the nozzle exit to the diffuser throat at 7.086 inches x 7.086 inches. From the throat, the subsonic diffuser plates each diverged at an angle of 6° (with maximum throat opening) from the tunnel centerline for an axial distance of 20.000 inches or 2.82 H at which point the adjustable diffuser ends. The transition section started 36 inches from the end of the adjustable diffuser. Over this length the duct had a constant cross-section of 7.086 inches x 11.515 inches.

6. Figure 2 shows the two scavenge-scoop configurations. The only difference between them was the

PERFORMANCE OF A CONVERGING-DIVERGING WIND TUNNEL
DIFFUSER IN THE PRESENCE OF A SCAVENGING SCOOP

I. INTRODUCTION

1. The idea of an oblique shock diffuser was initiated at NOL in 1946 by Kurzweg. In 1949 a "wedge type" diffuser was designed and incorporated into the NOL 18 x 18 cm Aerophysics Tunnel No. 3 (reference a). Kurzweg, in reference (b), describes the first above pitot recovery obtained with this diffuser at $M = 2.48$. Subsequent testing with this diffuser reported in reference (c) by Diggins and Lange resulted in diffuser end pressures ranging up to 1.8 times the pitot pressure in the test section at $M = 4.92$.

2. Being mindful of the diffuser experience and facilities available at NOL, Sverdrup and Parcel, Inc., through the Air Force, requested NOL to investigate a variable area diffuser incorporating a scavenging scoop. This is a scale model of the Air Force's Arnold Engineering Development Center's Supersonic Propulsion Wind Tunnel diffuser. The PWT will be used for testing full scale, operating ram jet and turbo-jet power plants. To avoid excessive contamination of the tunnel air the engine exhaust gases will be scavenged by a scoop mounted in the tunnel diffuser.

3. The power requirements for such a large tunnel are necessarily very large. Consequently, power savings which may be obtained by a diffuser are extremely important. Much information is available concerning the performance of highly efficient diffusers (reference b, c, d, and e) but neither these data nor the existing theory were adequate to predict the effect of the scavenge scoop on diffuser performance. To answer this question an investigation was conducted in the continuous NOL 18 x 18 cm Aerophysics Tunnel No. 3, the results of which are presented herein.

length of the inlet section. The scoop inlet was in the diffuser entrance cross-section in the two cases investigated, namely $l/H = 2.12$ and $l/H = 3.36$, which necessitated the different length scoop inlet sections. Ten percent of the impinging flow was scavenged by the scoop whose inlet diameter was 2.435 inches. The scavenged flow was removed through the hollow supporting airfoil and tunnel wall into an eight inch suction line. Figure 3 is a photograph showing the scoop model with the long inlet section installed in the tunnel. Figure 4 is a similar photograph showing the scoop with the short inlet section. The large pipe dominating the right side of Figure 5 is the eight-inch suction line through which the scavenged flow was removed from the tunnel. The smaller pipe is the chamber suction line.

7. During this investigation four of the six vacuum pumps normally used for operating the tunnel were used in series to remove the scavenged flow. The tunnel was operated using one to four of the compressor stages, depending upon tunnel Mach number, normally used for operating the continuous 40 x 40 cm Aeroballistics Tunnel No. 2.

III. TEST PROCEDURE

8. After having suction on the scoop the test procedure for each Mach number was as follows:

a. Determination of the starting pressure ratio P_{sphere}/P_0

(1) For each of a series of progressively smaller throat openings the end pressure was lowered until supersonic flow was established in the test section as determined from observation of the schlieren. P_{sphere} was read at the instant flow was established.

b. Determination of the pressure recovery P_{0E}/P_0 or P_{0E}/P_p

(1) Supersonic flow was established in the test section. For each of a series of progressively smaller throat openings the end pressure was raised until flow broke down in the test section as determined from observation of the schlieren. P_{0E} was

read at the instant flow was broken down.

c. Measurement of the diffuser sidewall static pressure

(1) Supersonic flow was established in the test section. The diffuser throat was closed to that opening which would result in optimum pressure recovery. The end pressure was adjusted so that the end pressure ratio (P_{sphere}/P_{0E}) was much smaller than one. This ratio was P_{opt} held constant and the diffuser sidewall static pressure measured.

(2) The above was repeated with one exception. The end pressure was adjusted so that the end pressure ratio closely approached one.

d. Schlieren photographs of the flow were taken at three or four stations along the tunnel. These photographs were made with the optimum diffuser throat opening and a constant end pressure ratio much less than one.

9. Measured quantities and instrumentation

Quantity	Means of Determination	Accuracy
Average Mach number	Nozzle calibration curves	± 0.01
Supply temperature	Precision Hg Thermometer	$\pm 0.1^{\circ}\text{C}$
Atmospheric pressure	Barometer	± 0.05 mm Hg
Dew point	G.E. Dew-point indicator	$\pm 0.5^{\circ}\text{C}$
Pressure drop across the drier	Differential Hg manometer	± 0.05 mm Hg
Static pressures between 0-30 mm Hg abs.	Differential Hg manometer	± 0.05 mm Hg
Sphere end pressure	Differential Hg manometer	± 0.05 mm Hg
Diffuser throat opening	Automatic counter	± 0.005 in.

10. At the higher Mach numbers some difficulty was originally encountered with tunnel leakage. It was found that leakage around the nozzle blocks and jet plates (plates joining the nozzle exit and diffuser entrance) was most detrimental to the diffuser's performance. In addition to completely regasketing the tunnel, suction was applied to the chambers above and below the upper and lower nozzle blocks and jet plates, respectively, to reduce to a negligible amount leakage of atmospheric air into the tunnel flow. The static pressure in these chambers (Figures 3 and 4) was maintained through the use of suction at a value slightly higher than the free stream static pressure. On the figures and in the following text the use of the phrase "test chamber suction" should not be confused with the suction through the scoop and simply means that suction was applied to the chambers above and below the test section.

IV. RESULTS

11. Figures 6, 7 and 8 have been included as an aid to the understanding and interpretation of the experimental data. Figure 6 shows the maximum free duct cross-section along the diffuser. This condition existed when the diffuser throat was at its most open position (supersonic diffuser plates parallel). The free duct cross-section was any diffuser cross-section from which had been subtracted the corresponding scoop cross-section.

12. Figure 7 shows the diffuser entrance half-angle θ and the subsonic diffuser half-angle ϕ as a function of the diffuser area ratios. Both θ and ϕ are measured with respect to the tunnel centerline. One notices immediately that the subsonic diffuser half angle is larger than is desirable even at an area ratio of one and becomes larger with decreasing area ratio. When the diffuser throat is at its maximum opening the subsonic diffuser half angle is approximately 6° and the effective half angle, based on the free duct area in the planes of the diffuser throat and subsonic diffuser exit, is 4° . This unfavorable situation existed because of a total length restriction placed upon the adjustable diffuser. There are two curves for the diffuser entrance half-angle;

one for the long supersonic diffuser whose $l/H = 3.36$ and the other for the short supersonic diffuser whose $l/H = 2.12$.

13. The test section Reynolds number is plotted versus Mach number in Figure 8. The Reynolds number is based upon; $H = 18$ cm, $P_0 = 750$ mm Hg absolute and $T_0 = 15^\circ\text{C}$. At $M = 1.86$ the Reynolds number is 2.5 million and ranges down to 0.6 million at $M = 4.92$.

14. Starting pressure ratio as a function of diffuser area ratio for each of the Mach numbers investigated is plotted in Figure 9. It is significant that the tunnel may be started (supersonic flow established) at a more favorable pressure ratio with the diffuser partially closed than with the diffuser wide open. This effect becomes more pronounced with increasing Mach number. The vertical tangents to the left of the curves indicate that further closing of the diffuser throat would entirely prevent establishing flow. The highest starting pressure ratios and minimum starting area ratios are slightly lower than, but compare favorably with, the clear tunnel data of reference (c) indicating the absence of a large effect due to the scoop on these parameters. The $l/H = 3.36$ diffuser is the better of the two configurations considered. Comparison of the data taken with and without chamber suction points out the absence of, or negligible effect of, tunnel leakage at Mach numbers 3.24 and below.

15. Figure 10 shows how the minimum starting area ratio decreases with increasing Mach number. Comparison of the scoop data with the data of reference (c) with optimum throat location and model shows that flow may be established with the scoop at a smaller area ratio than with the model of reference (c). This may be explained by the fact that suction flow is established through the scoop prior to starting the tunnel and that the shock loss from the model is greater than from the scoop inlet. Over the Mach number range investigated, it was possible to establish supersonic flow at a smaller area ratio with the $l/H = 3.36$ configuration than with the $l/H = 2.12$ configuration. At $M = 4.30$ and $M = 4.92$ the adverse

effect of tunnel leakage on the minimum starting area ratio is clearly pointed out by comparison of the suction and non-suction data.

16. Comparison of the scoop diffuser minimum operating area ratio data with the data of reference (c) for clear tunnel and optimum throat location is made in Figure 11. As would be expected the scoop values are slightly higher than those of reference (c). The curves parallel one another up to about $M = 3.00$ at which point the scoop data breaks away. This break away may be explained by the large increase in the ratio of the boundary-layer thickness to diffuser throat opening with the scoop at the higher Mach numbers and also by flow separation which occurs in the supersonic diffuser at the two highest Mach numbers. The $l/H = 3.36$ configuration may be operated at smaller diffuser area ratios than the short configuration. Here again the adverse effect of tunnel leakage is pointed out by comparison of the suction and no suction data at $M = 4.30$ and $M = 4.92$.

17. Figures 12 through 17 inclusive are plots of pitot pressure recovery versus diffuser area ratio for each of the Mach numbers investigated. Higher recoveries are achieved at every Mach number with the $l/H = 3.36$ configuration than with the $l/H = 2.12$ configuration. Wherever possible comparison of the scoop data is made with the data of reference (c) with optimum throat location and with model (a 60° total angle cone of 3 cm base diameter on a circular arc support with a total projected area of $0.027 H^2$). As is expected, with increasing Mach number the scoop data are increasingly lower as compared to reference (c). The effect of chamber suction or the absence of tunnel leakage has a large effect at the two higher Mach numbers, approximately 20% improvement in pitot pressure recovery.

18. Optimum pitot pressure recovery is plotted as a function of Mach number in Figure 18. The three uppermost curves are comparison data from reference (c). Starting from the top, they are: (1) optimum recovery with optimum throat location and clear tunnel; (2) optimum recovery with the throat located at $l/H = 3.36$ and clear tunnel; and (3) optimum

recovery with optimum throat location with the model described in the preceding paragraph. The optimum recoveries achieved with the scavenge scoop-diffuser combination are naturally lower than the comparable data from reference (c). The lowered recoveries with the scoop are probably due to increased friction losses, unfavorable throat location, boundary-layer separation in the supersonic diffuser and an excessively large subsonic diffuser angle. The scoop data curves between $M = 1.86$ and $M = 3.24$ exhibit the same trend as the reference (c) data; however, there is a sharp drop-off at the two higher Mach numbers. This is due to boundary-layer separation and the excessively large subsonic diffuser angle. A less pronounced drop at the higher Mach numbers is to be expected in a larger tunnel operating at higher Reynolds numbers.

19. Figure 19 has the data of Figure 18 replotted. The end pressure is now referred to the supply pressure and this ratio decreases rapidly with increasing Mach number. This is to be expected since the shock losses increase rapidly with increasing Mach number. The curve for an $l/H = 3.36$ is drawn through the "with suction" data while the curve for an $l/H = 2.12$ is drawn through the "without suction" data. This fact is pointed out to save confusion.

20. The diffuser sidewall static pressure distributions are given in Figures 20 through 31. All of the data were taken with chamber suction except that for an $l/H = 2.12$ at $M = 1.86, 2.48, 2.83$ and 3.24 , which are presented in Figures 20, 22, 24, and 26. The data were taken with a diffuser area ratio at which optimum pressure recovery can be achieved. In most cases two distributions were measured for each configuration and Mach number. One distribution was measured with an end pressure ratio ($P_{\text{sphere}}/P_{0E_{\text{opt}}}$) close to one (near flow breakdown). The other distribution was measured with an end pressure ratio much less than one.

21. Consider first the distributions taken with an end pressure ratio nearly one. The static pressure ratio is higher at the diffuser throat and at the most downstream measuring station with

the $1/H = 3.36$ configuration than with the $1/H = 2.12$ configuration, i.e., Figures 20 and 21, 28 and 29, and 30 and 31. Noteworthy also is the greater static pressure rise accomplished in the supersonic diffuser as compared to the subsonic diffuser.

22. The static pressure distributions measured with an end pressure ratio much less than one in the supersonic diffuser are very similar and in many cases identical to those measured with the high end pressure ratio. The cases in which the high end pressure data are above the low end pressure data immediately upstream of the diffuser throat are explained by the upstream travel of the higher subsonic diffuser pressure through the separated boundary layer. In the subsonic diffuser the static pressure suddenly drops due to the re-expansion of the flow. The erratic behavior of the data in that section is explained by flow separation and reattachment.

23. The static pressure distributions corroborate and clarify the results of the pressure recovery measurements. The $1/H = 3.36$ configuration is superior to the $1/H = 2.12$ configuration at all Mach numbers investigated.

24. Schlieren photographs of the flow at $M = 1.86$, 2.48, 3.24, 4.30 and 4.92 are presented in Figures 32, 33, 34, 35, and 36, respectively. The individual pictures forming the composite picture of one configuration were all taken at the same diffuser area ratio and end pressure ratio. The end pressure ratio was always much less than one. The dark outline about the composite picture indicates the contour of the diffuser plates, and the diffuser inlet and throat are pointed out. The pictures show clearly; (1) the boundary-layer growth, (2) the shock intersection tripping the laminar boundary layer and possibly causing separation upstream of the interaction, (3) the oblique shock pattern, (4) the large expansion of the flow immediately downstream of the diffuser throat, and (5) that the flow is supersonic in the subsonic diffuser. The last two points corroborate the results of the low end pressure ratio static pressure measurements in the subsonic diffuser and the previous statements regarding the inefficiency of the subsonic diffuser.

25. In Figure 36 the upper composite picture of the $l/H = 3.36$ configuration shows the diffuser throat closed until it strikes the model. The flow could not be choked in this case since the diffuser throat could not be closed further. This fact explains the absence of the vertical portion on the left end of the curve for the corresponding data in Figure 17.

26. The two schlieren photographs in Figure 37 show the effect of area ratio or changing the diffuser entrance angle on the flow in the supersonic diffuser at $M = 4.30$. It is particularly interesting to note the boundary-layer separation which occurs upstream of the shock wave intersection on the scoop in the lower picture.

27. Supersonic flow could not be established in the tunnel at any of the Mach numbers investigated without having suction on the scoop. Further, supersonic flow could not be maintained in the tunnel after stopping suction on the scoop.

V. CONCLUSION

28. The tunnel can be operated with the scavenge scoop installed. Supersonic flow can be established and maintained only when suction is applied to the scoop.

29. The presence of the scavenge scoop did not seriously affect the optimum starting pressure ratio or the minimum starting area ratio as compared to the tunnel clear data with optimum throat location. Further, the scavenge scoop diffuser combination as compared to the scavenge scoop with no convergence of the supersonic diffuser shows an improvement in starting pressure ratio which ranges from 0% at $M = 1.86$ to 24% at $M = 4.92$.

30. The presence of the scavenge scoop causes a marked reduction in the pressure recovery as compared to the recovery of the tunnel with 60° cone model. The lower recovery is probably due to the increased friction losses, the specified diffuser throat location as compared to the optimum throat location and the inefficient operation of the subsonic diffuser.

However, the improvement in pressure recovery with the scavenge scoop diffuser combination as compared to the scavenge scoop with no convergence of the supersonic diffuser ranged from 2% at $M = 1.86$ to 43% at $M = 4.92$. Improved recovery at the higher Mach numbers is to be expected in a larger tunnel operating at higher Reynolds numbers.

31. The comparison of optimum pressure recovery data at the higher Mach numbers with and without chamber suction shows that tunnel leakage can markedly reduce the diffuser pressure recovery.

32. The diffuser sidewall static pressure distributions point out that a reasonably good static pressure rise is being accomplished in the supersonic diffuser, even greater than is being accomplished in the subsonic diffuser.

VI. REFERENCES

- a. Henderson, Hayward W., "Naval Ordnance Laboratory 18 x 18 cm Supersonic Wind Tunnel - Design Criteria, Description of Tunnel, Operating Technique." NOLM 10379, Naval Ordnance Laboratory, White Oak, Silver Spring, Md., 3 August 1949.
- b. Kurzweg, H. H., "A Few Aspects of Future Supersonic Wind Tunnel Design and Test Techniques." U. S. Naval Ordnance Laboratory NOLR 1133, 29 June 1949.
- c. Diggins, J. L., and Lange, A. H., "A Systematic Study of a Variable Area Diffuser for Supersonic Wind Tunnels." NAVORD Report 2421, Naval Ordnance Laboratory, White Oak, Silver Spring, Md., December 1952.
- d. Neumann, E. P., and Lustwerk, F., "Supersonic Diffusers for Wind Tunnels." Jour. Applied Mech. 16, 2, 195, June 1949.
- e. Neumann, E. P., and Lustwerk, F., "High Efficiency Supersonic Diffusers," Jour. Aeronaut. Sci. 18, 6, 369-374, June 1951.

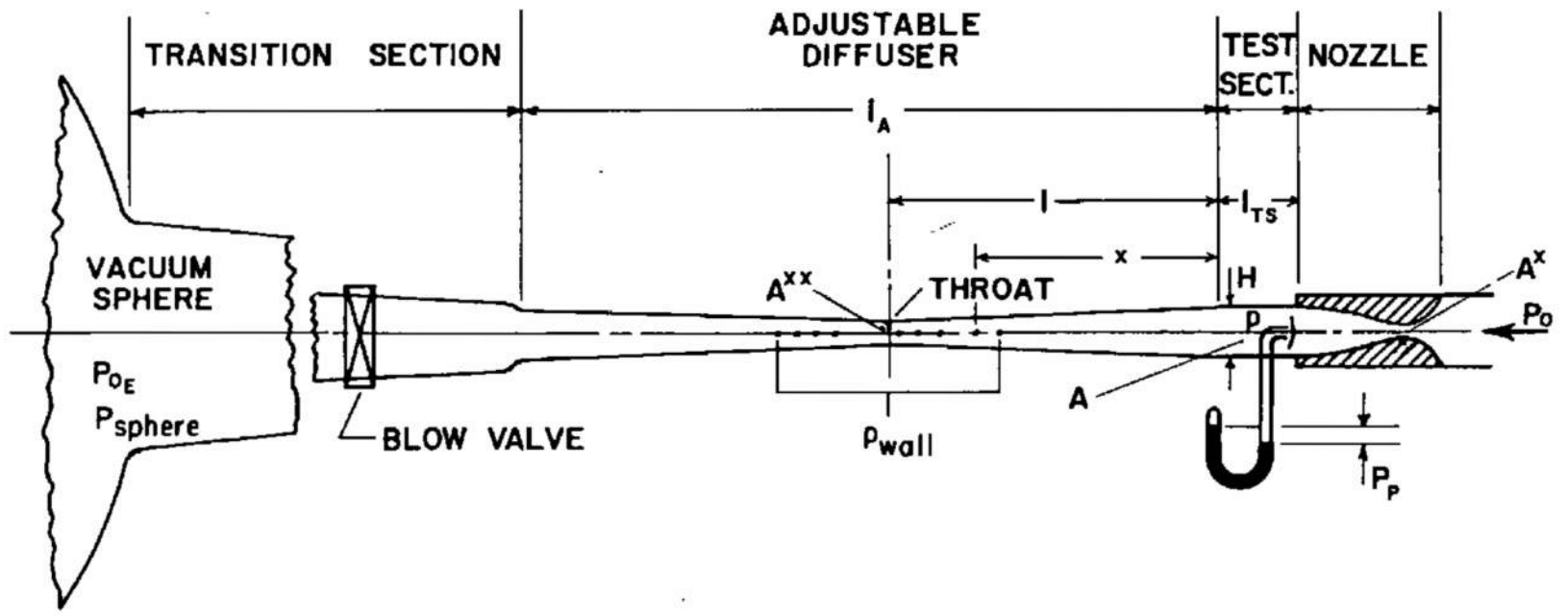


FIG. 1 DUCT CONFIGURATION, SCHEMATIC

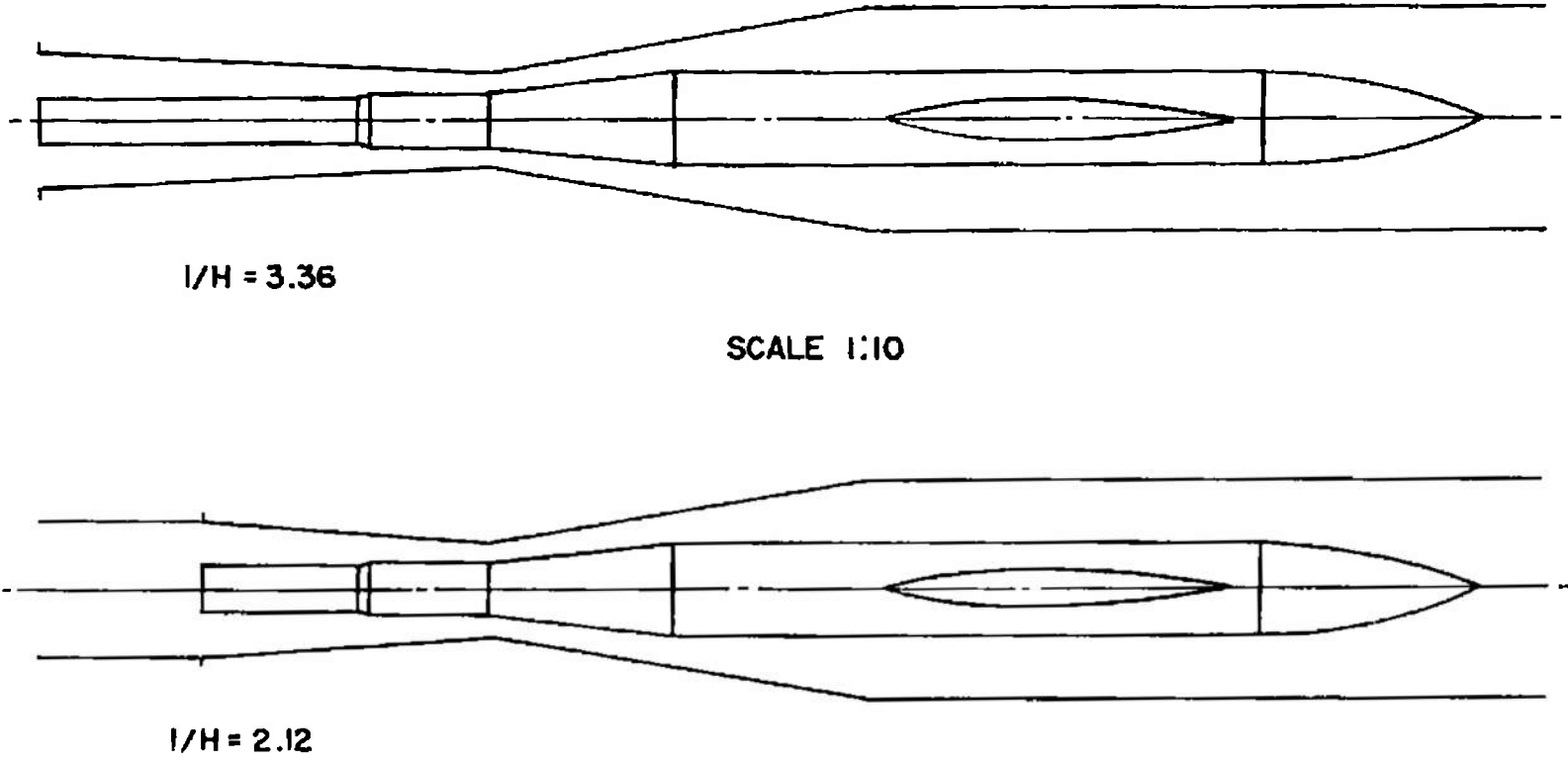


FIG. 2 SCOOP-DIFFUSER MODELS

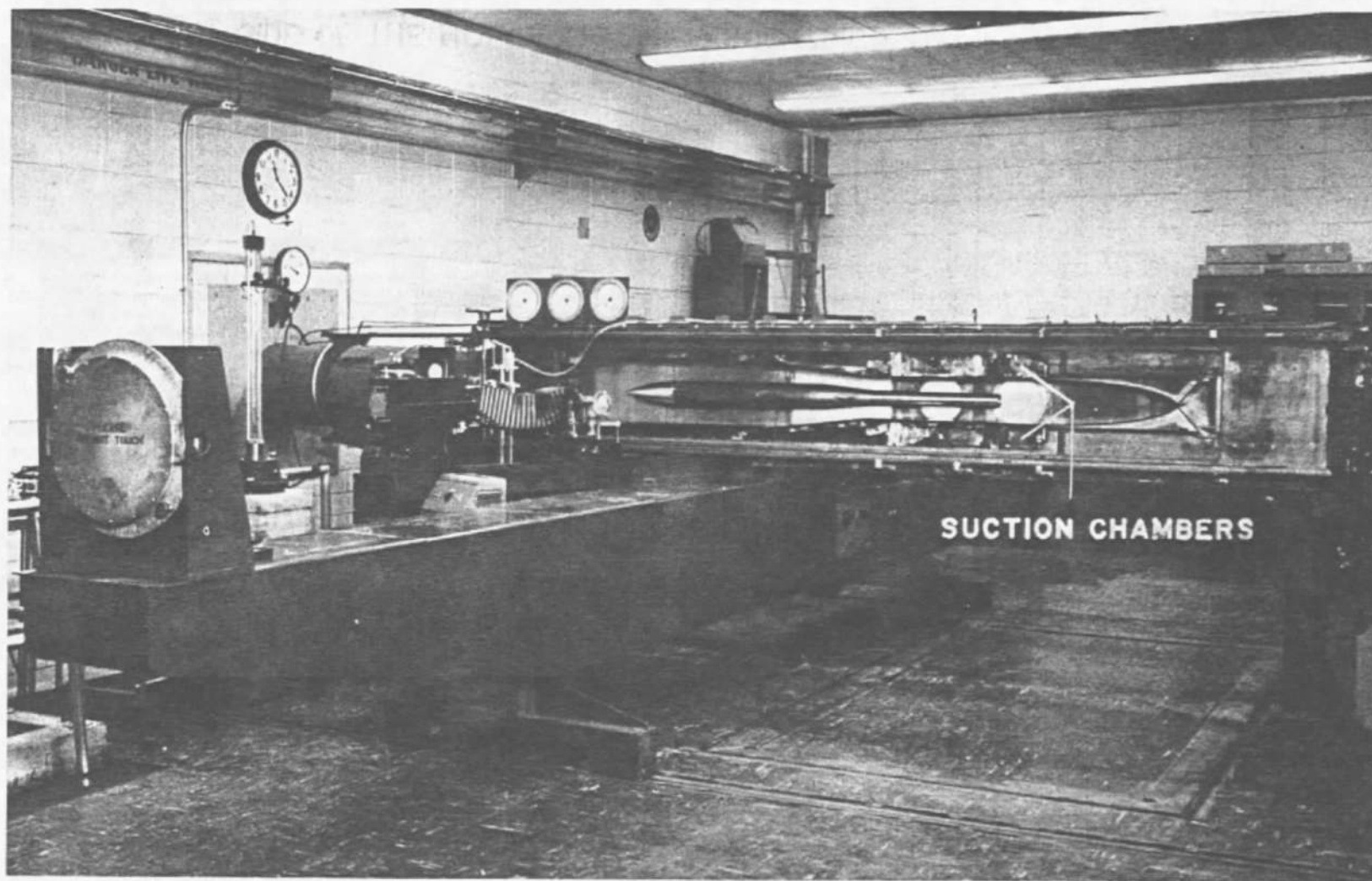
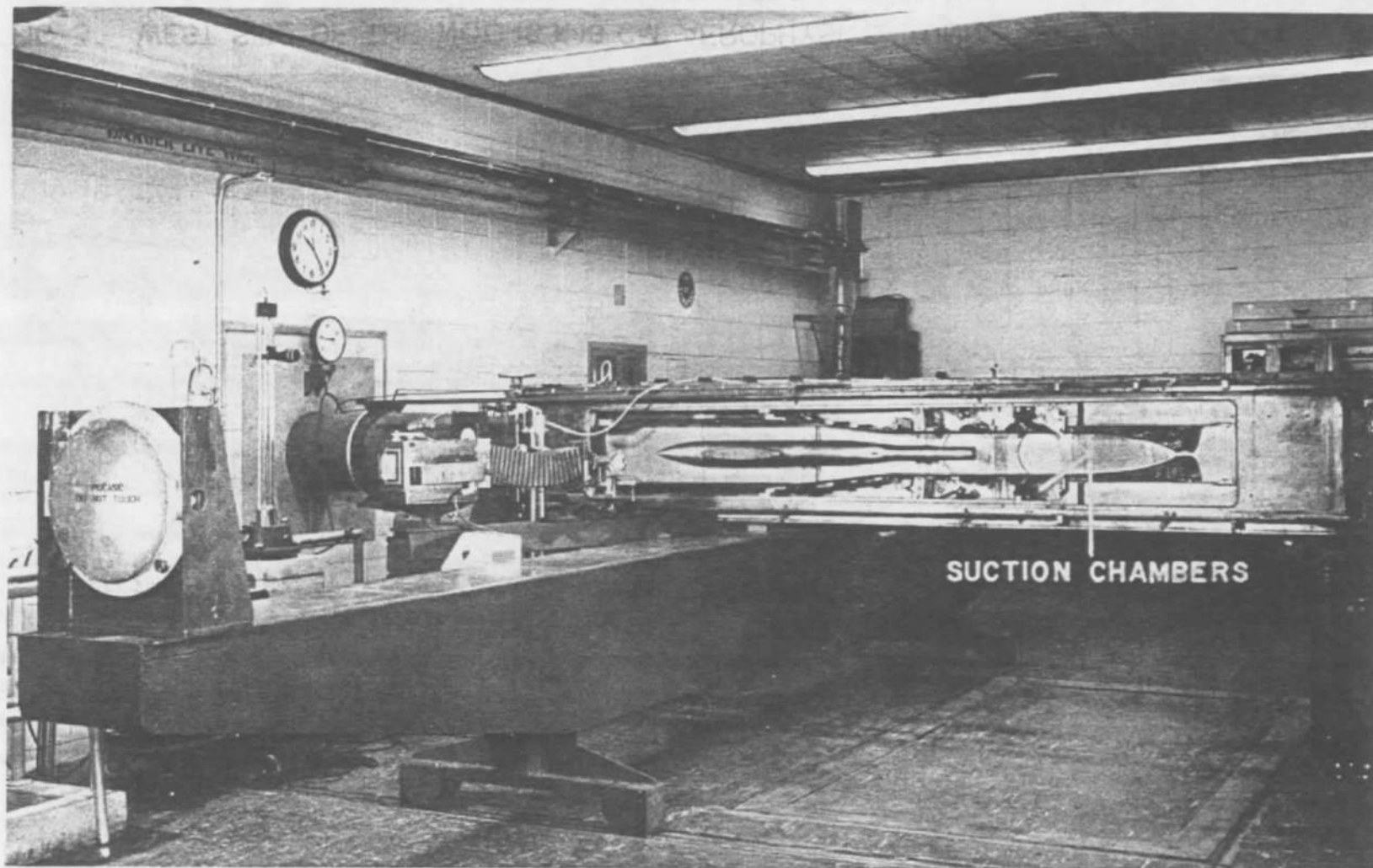
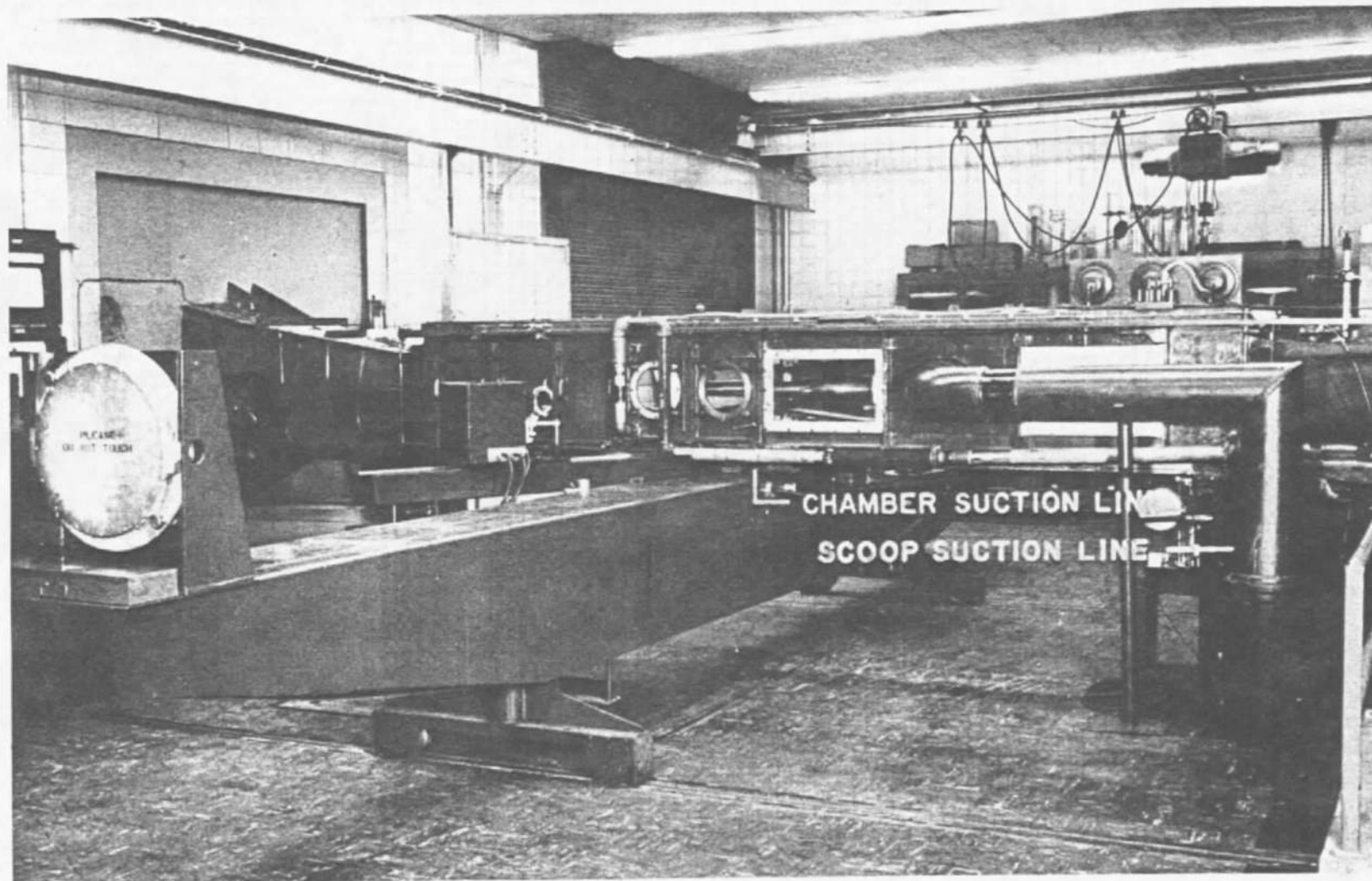


FIG. 3 WEST SIDE OF THE NOL 18 X 18 CM AEROPHYSICS TUNNEL NO. 3 WITH THE LONG SCAVENGING - SCOOP MODEL INSTALLED



NAVORD REPORT 3665

FIG. 4 WEST SIDE OF THE NOL 18 X 18 CM AEROPHYSICS TUNNEL NO. 3 WITH THE SHORT SCAVENGING - SCOOP MODEL INSTALLED



NAVORD REPORT 3665

FIG.5 EAST SIDE OF THE NOL 18 X 18 CM AEROPHYSICS TUNNEL NO.3 SHOWING THE TEST CHAMBER AND SCAVENGING-SCOOP SUCTION LINES

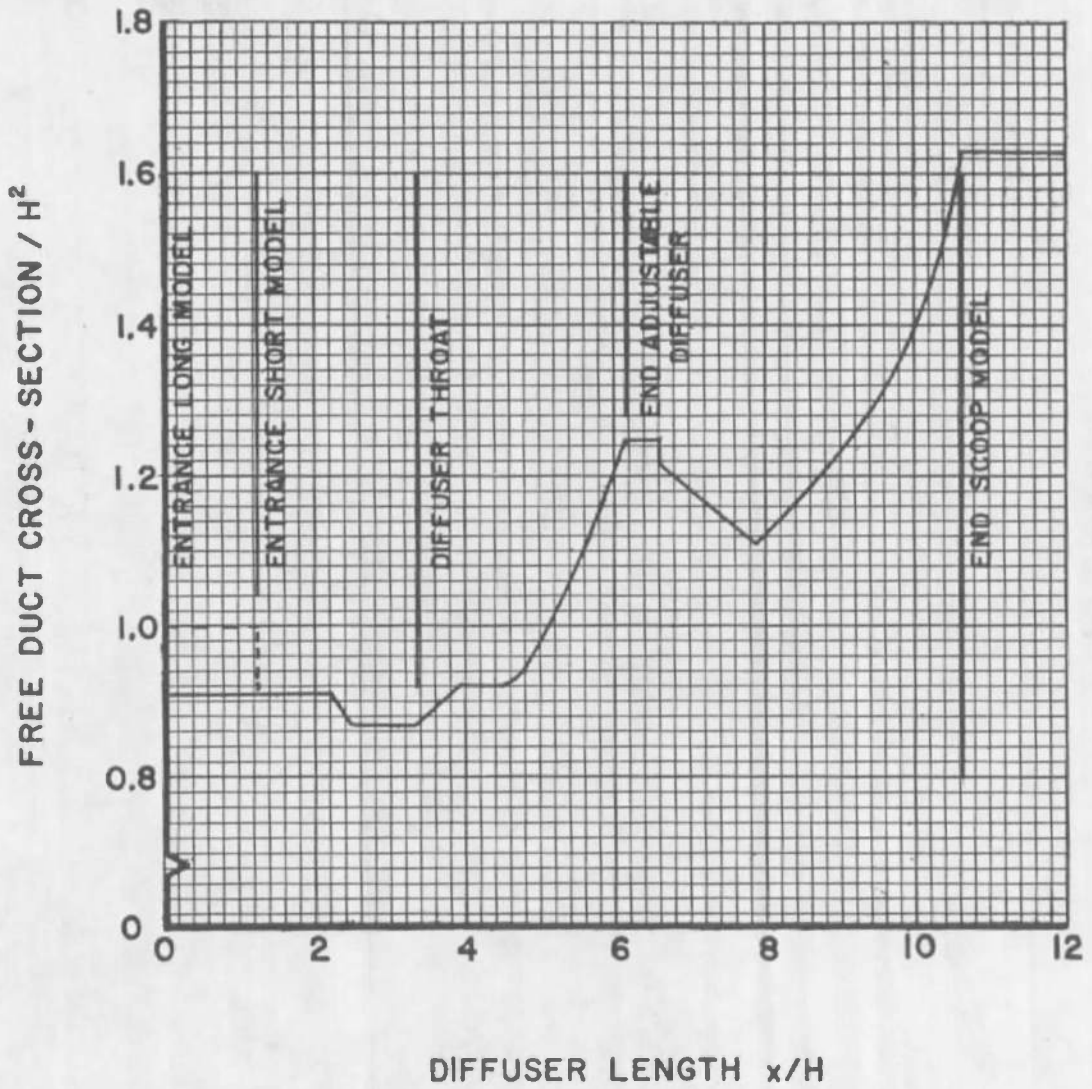


FIG. 6 MAXIMUM FREE DUCT CROSS-SECTION ALONG THE DIFFUSER

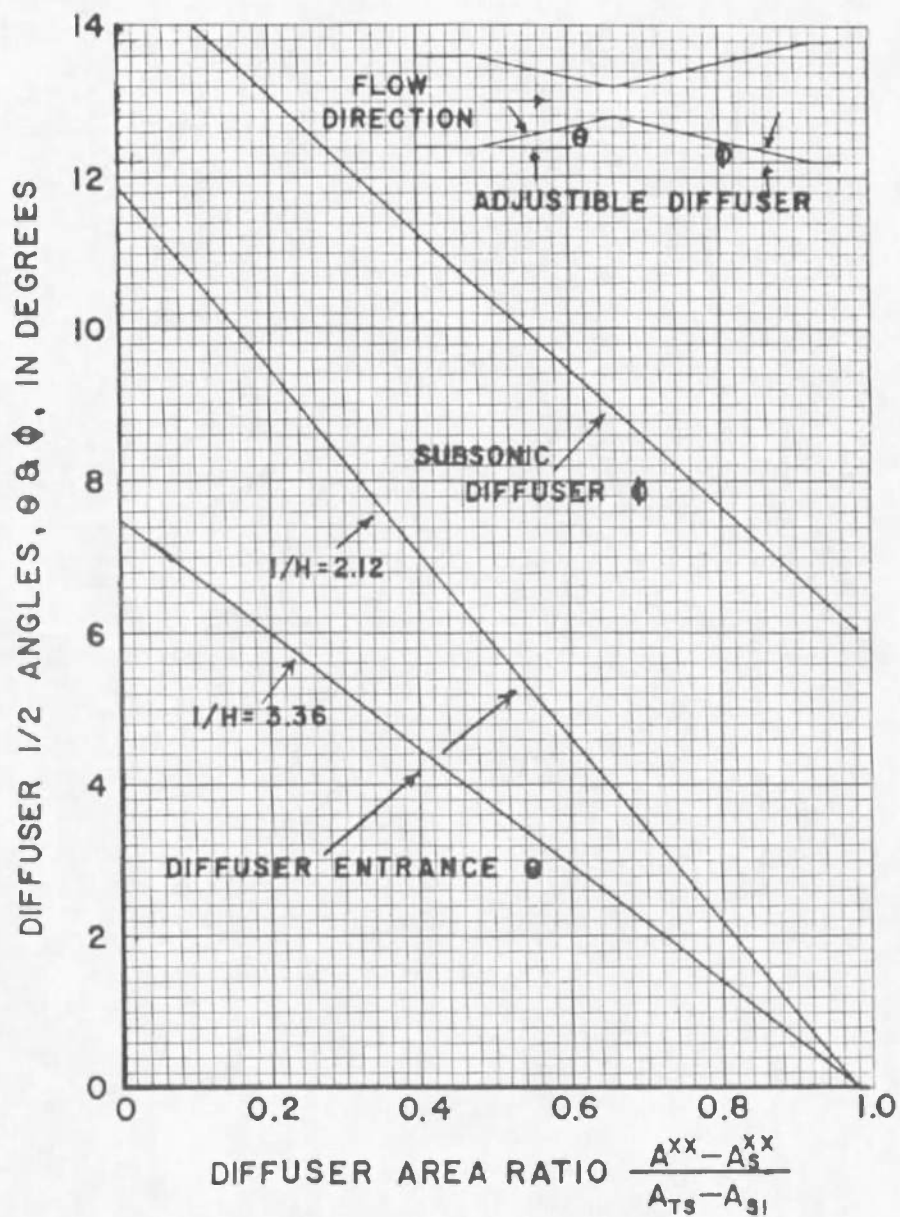


FIG. 7 DIFFUSER ENTRANCE 1/2 ANGLE & SUBSONIC DIFFUSER 1/2 ANGLE

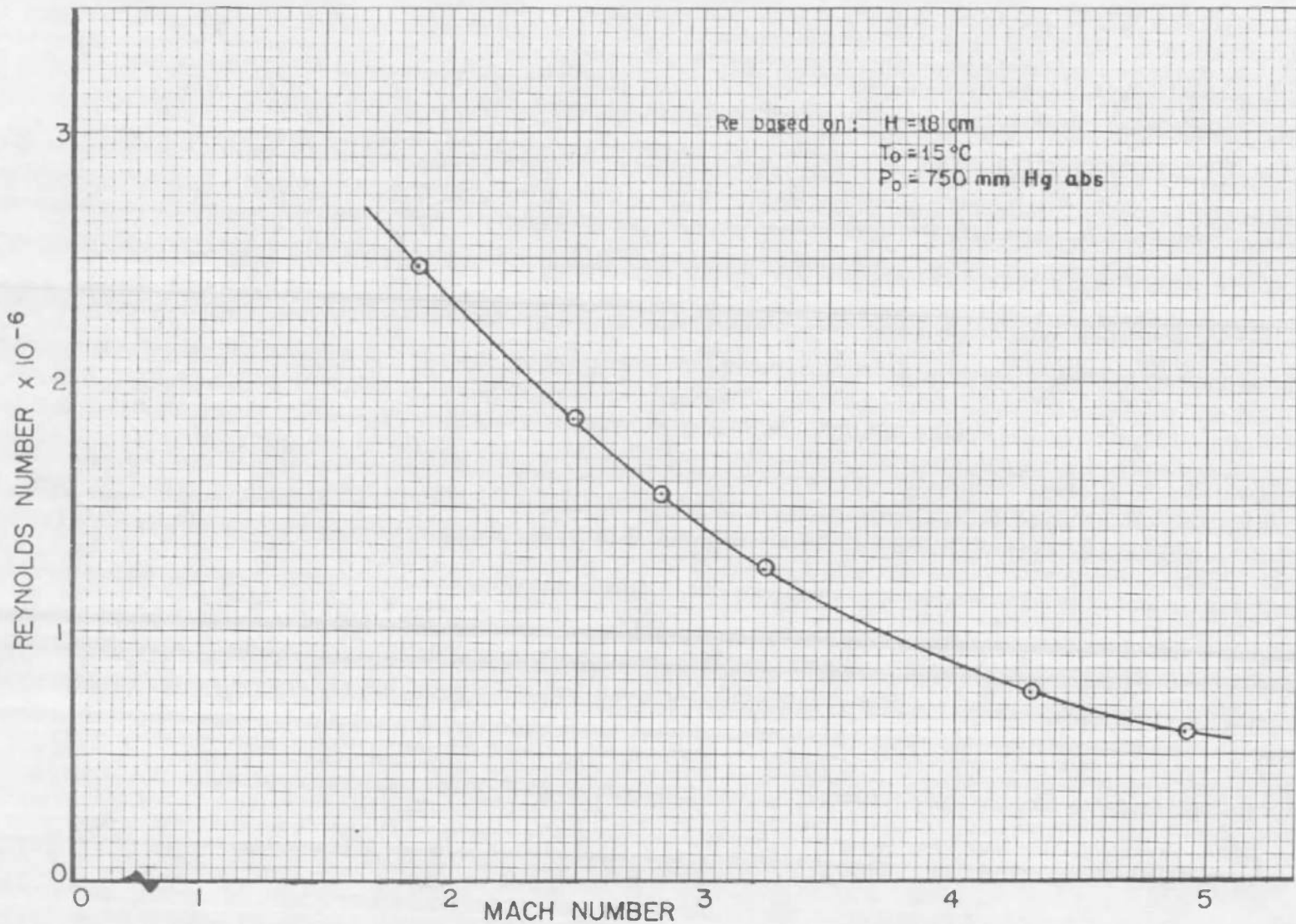


FIG. 8 REYNOLDS NUMBER VS MACH NUMBER

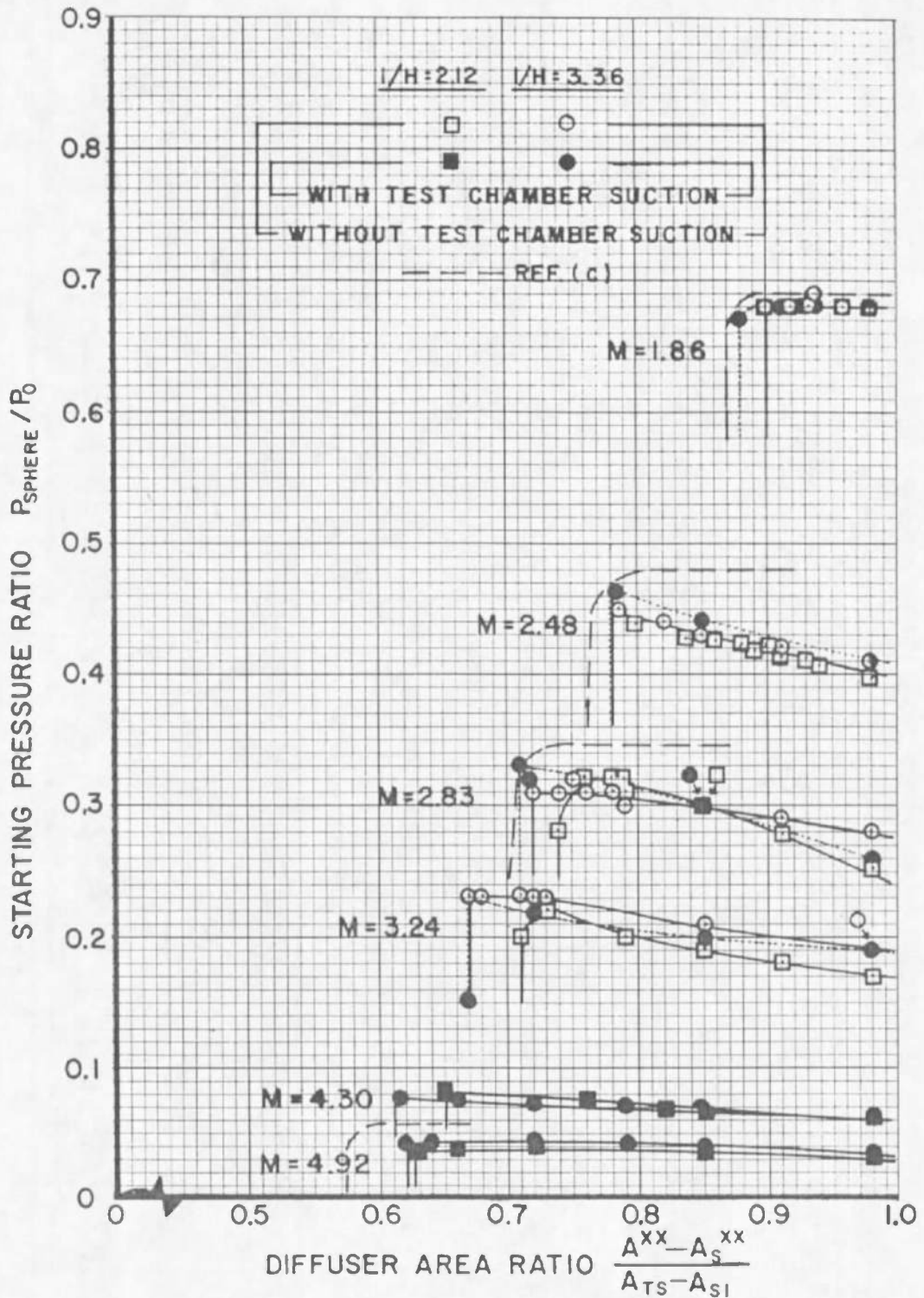


FIG. 9 STARTING PRESSURE RATIO VS
DIFFUSER AREA RATIO

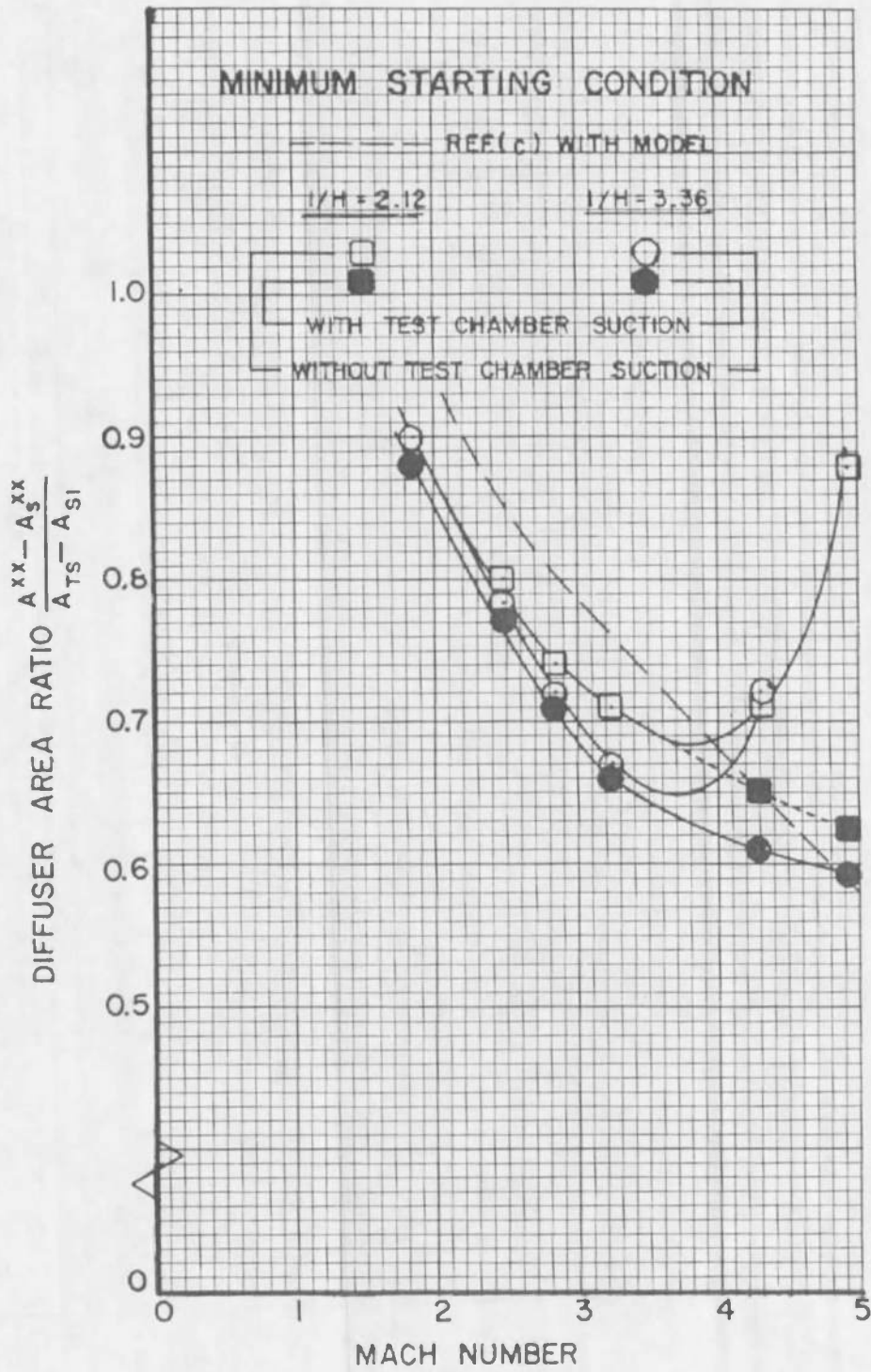


FIG. 10 MINIMUM STARTING AREA RATIOS

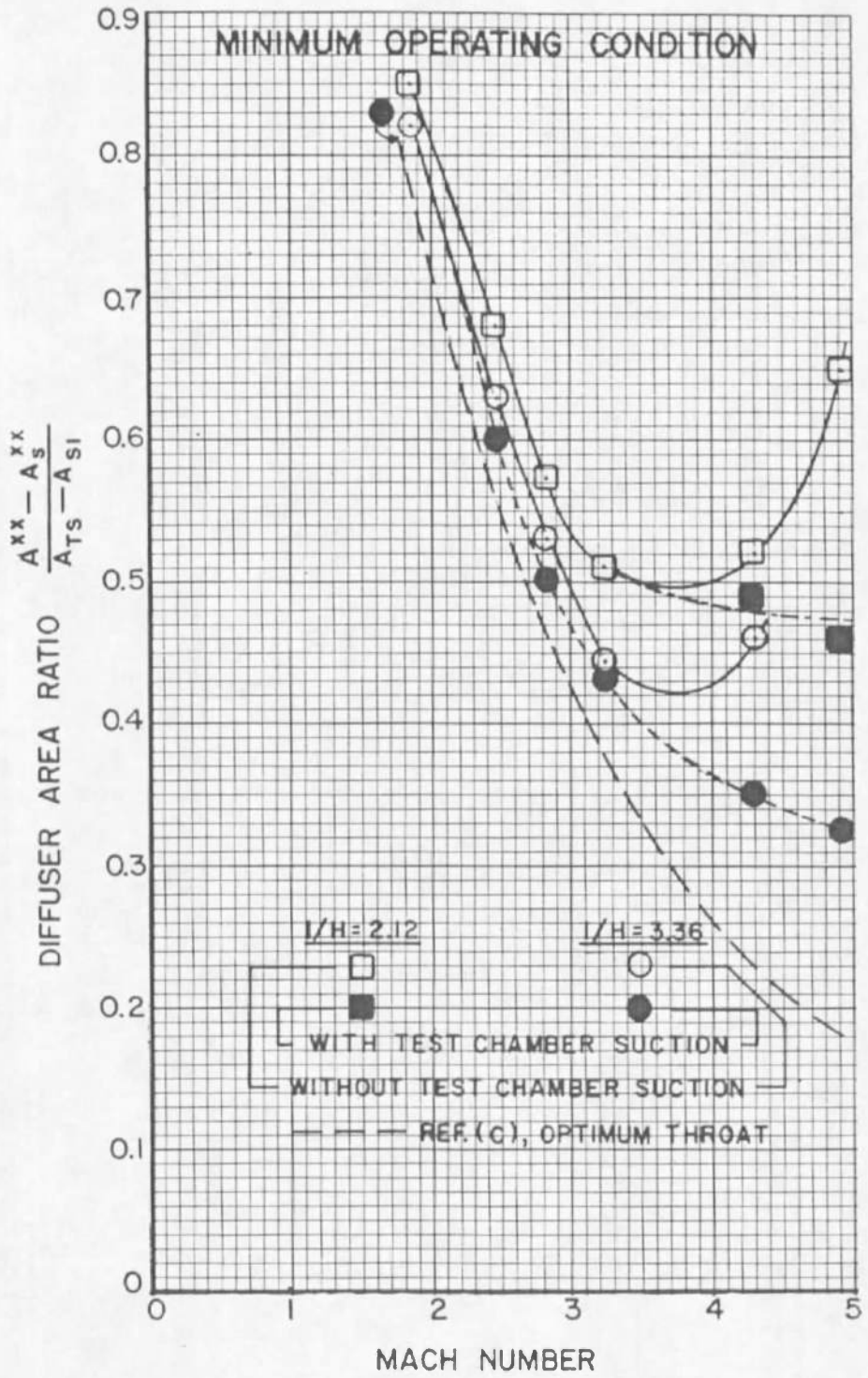


FIG. II MINIMUM OPERATING AREA RATIOS

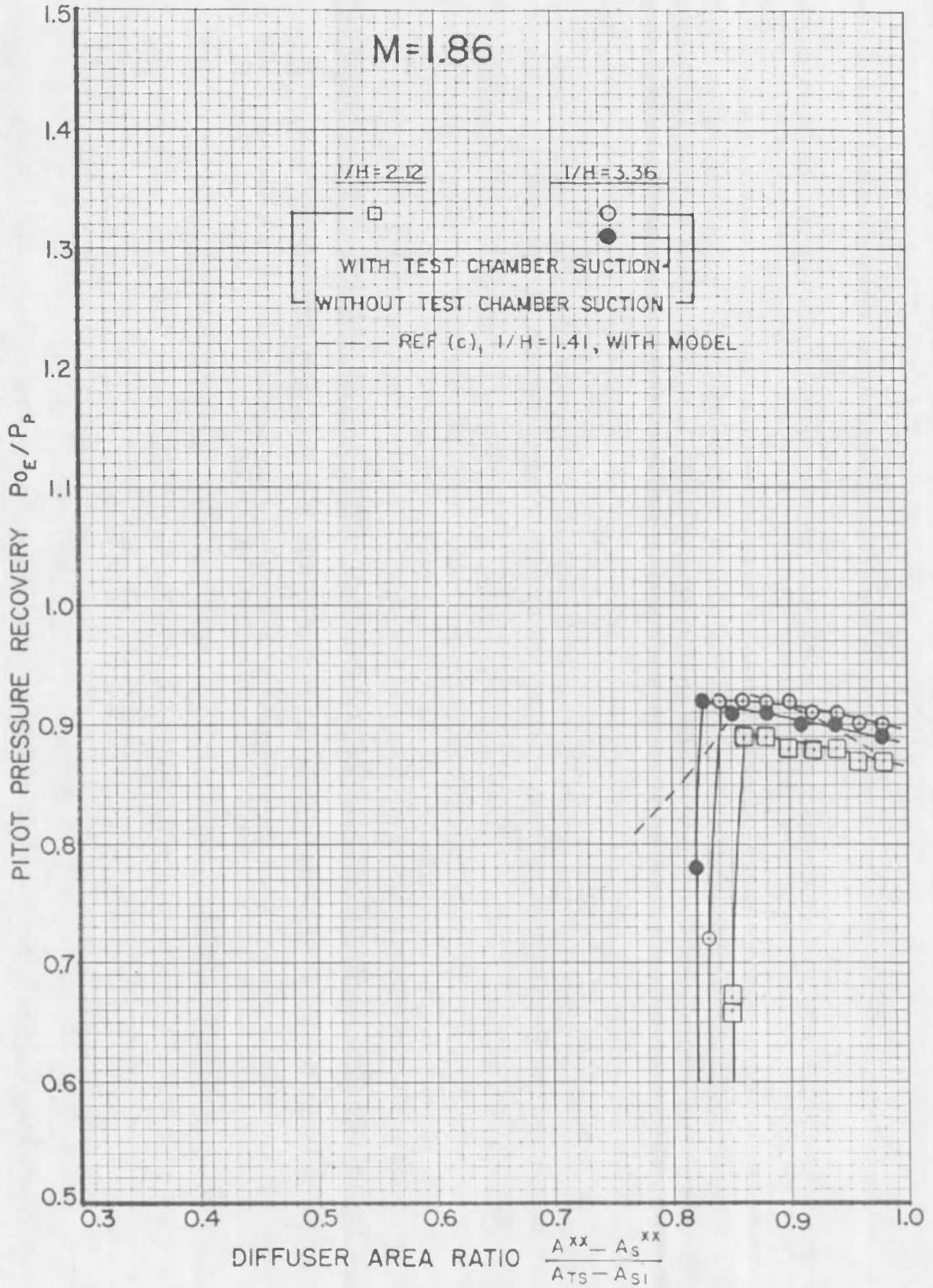


FIG. 12 PITOT PRESSURE RECOVERY

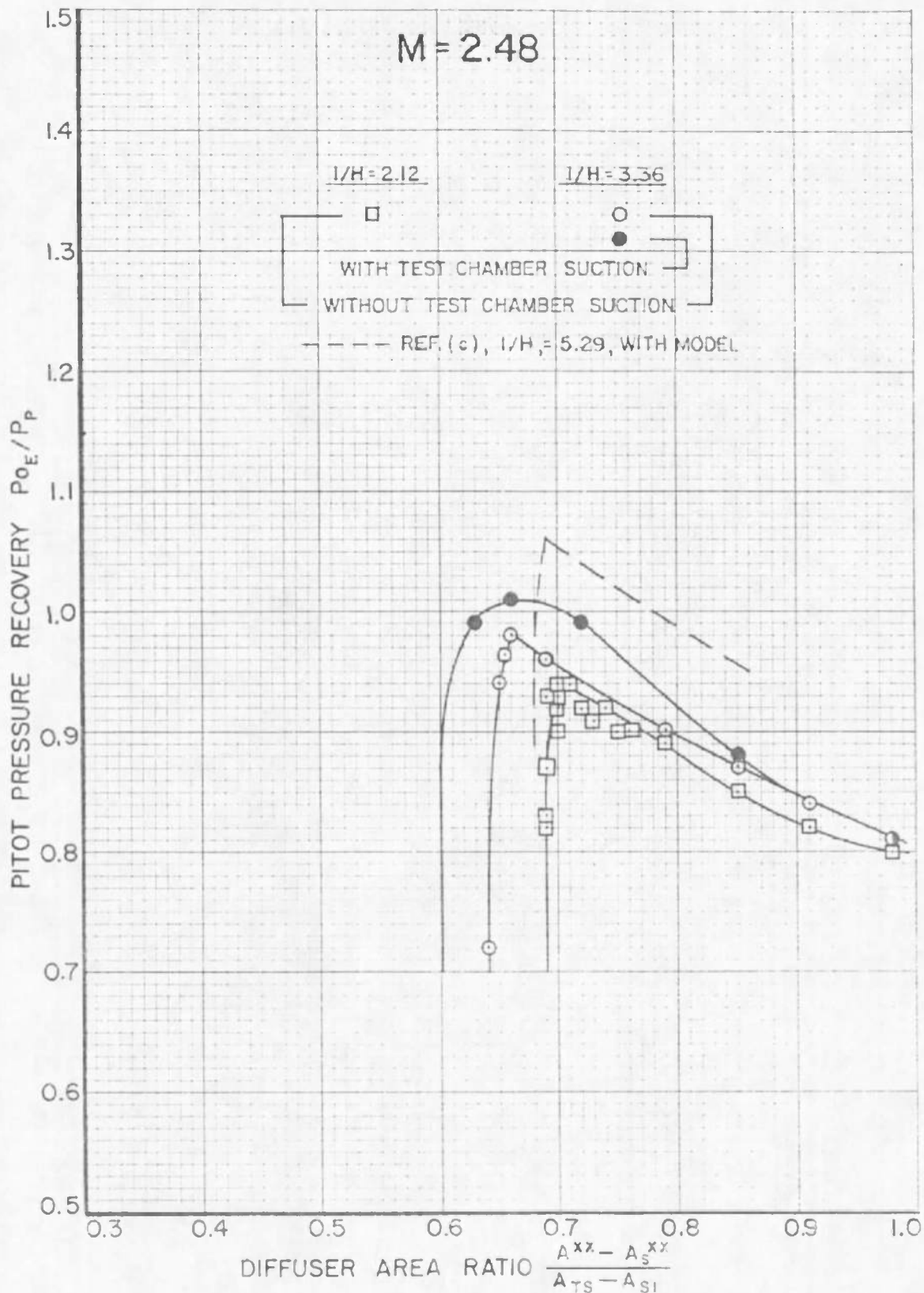


FIG. 13 PITOT PRESSURE RECOVERY

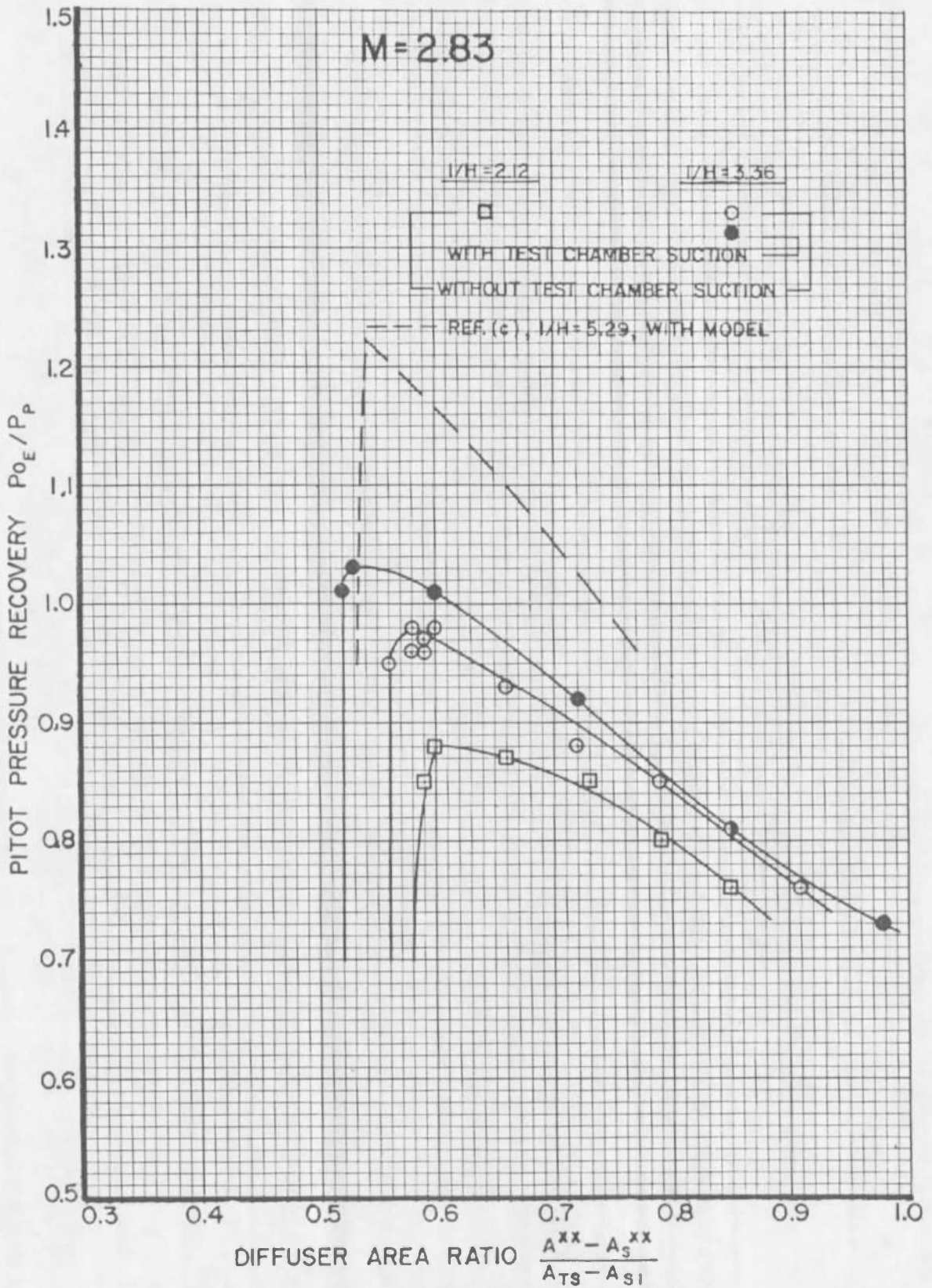


FIG. 14 PITOT PRESSURE RECOVERY

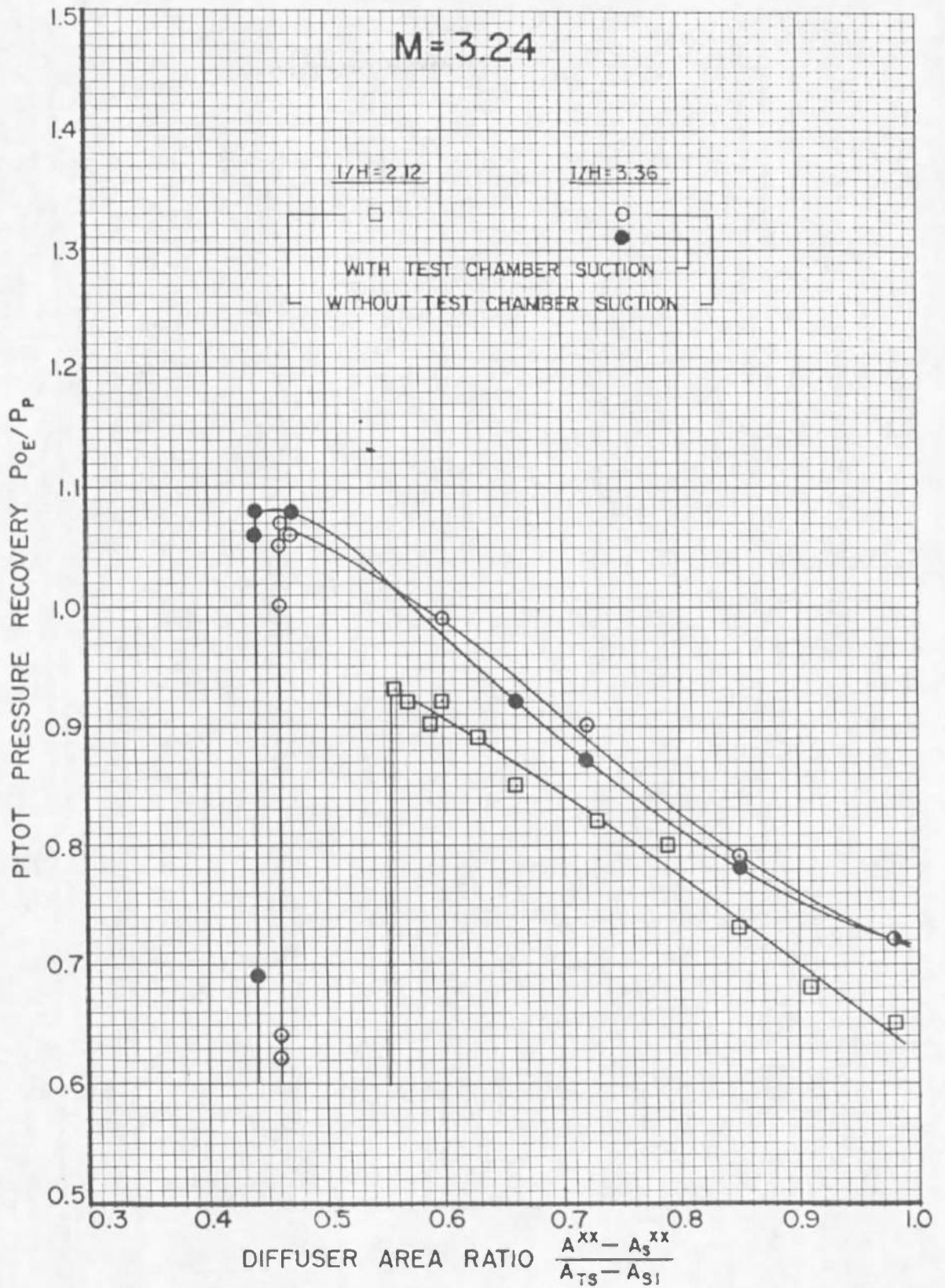


FIG. 15 PITOT PRESSURE RECOVERY

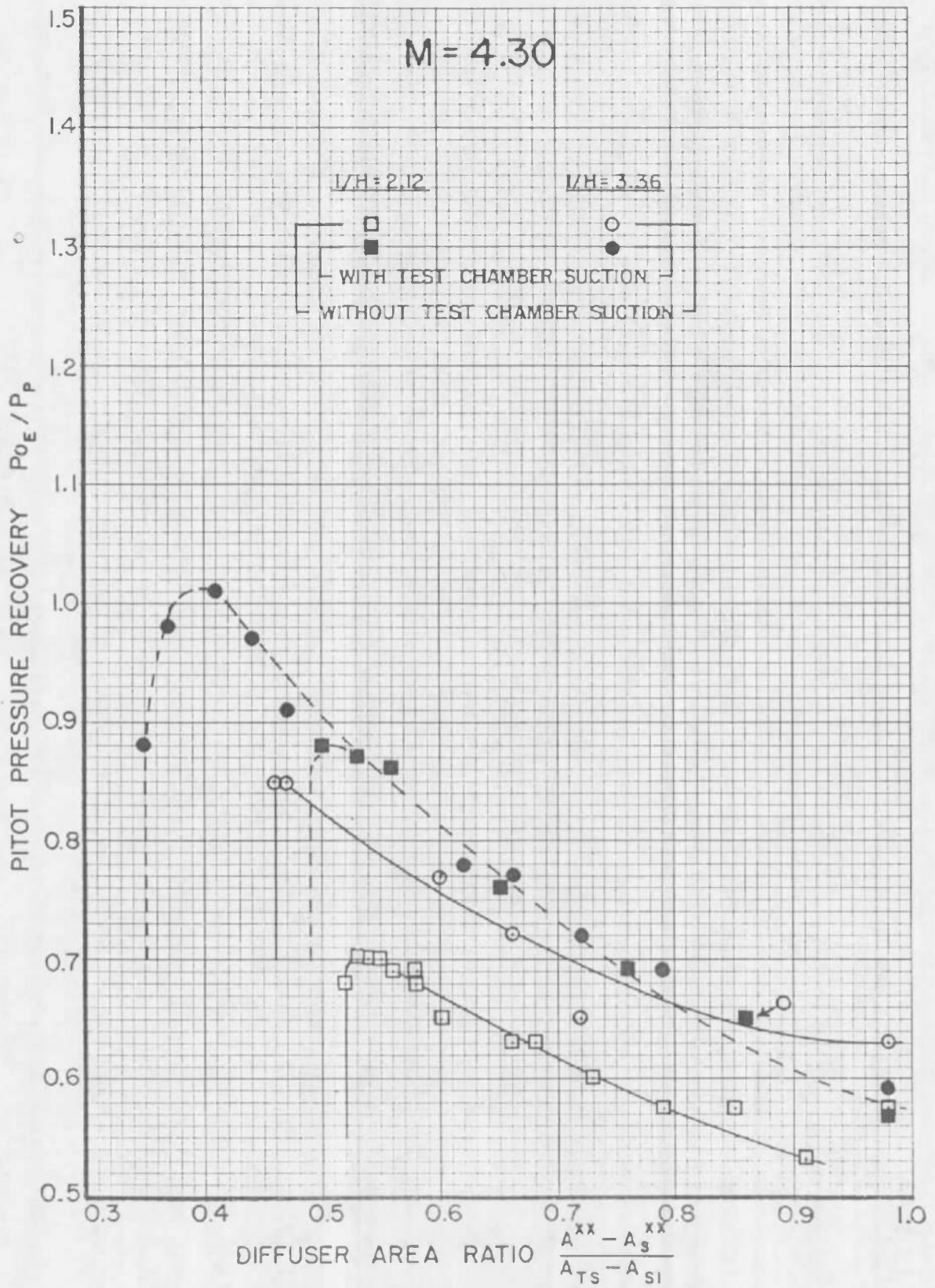


FIG. 16 PITOT PRESSURE RECOVERY

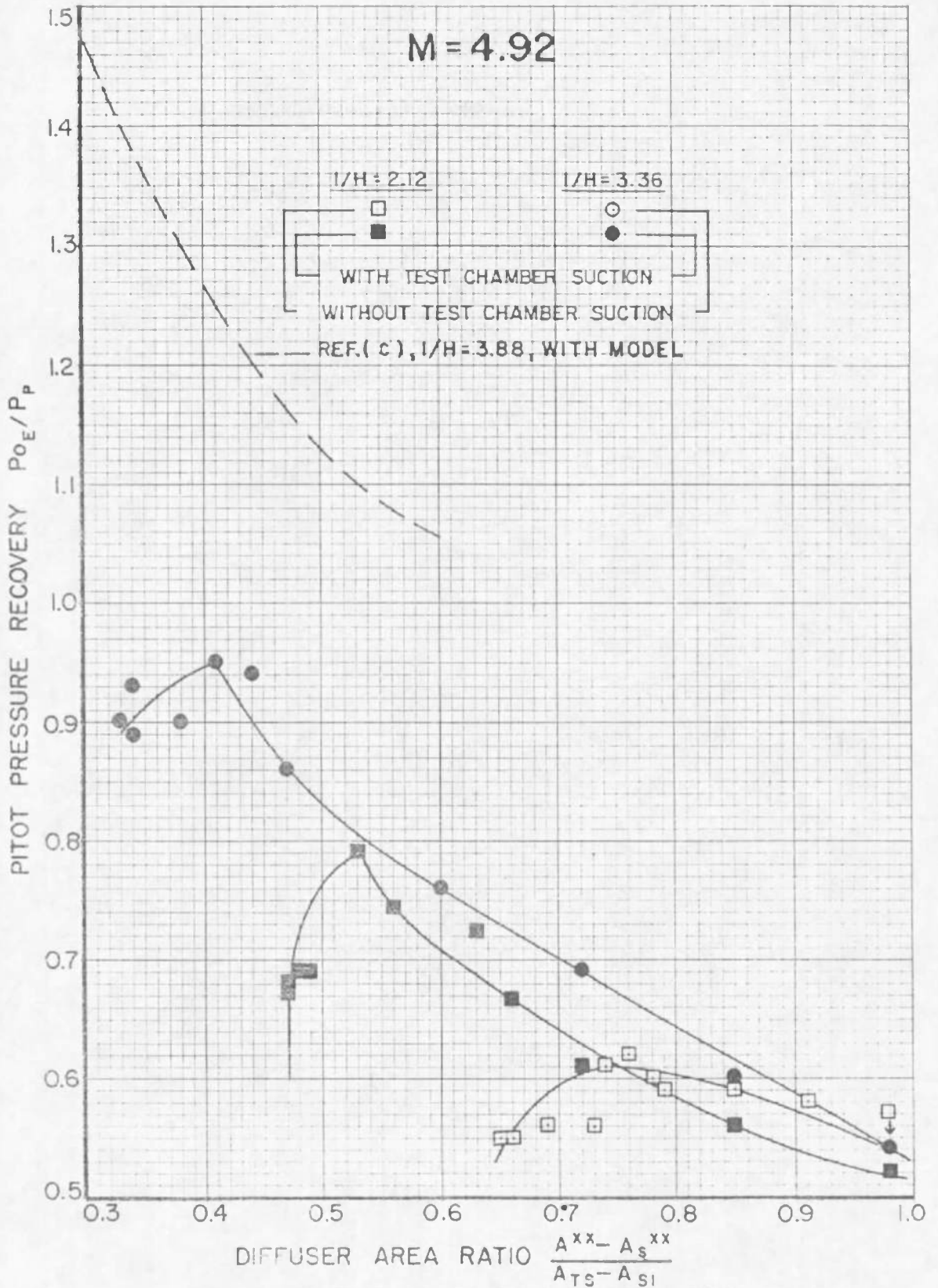


FIG. 17 PITOT PRESSURE RECOVERY

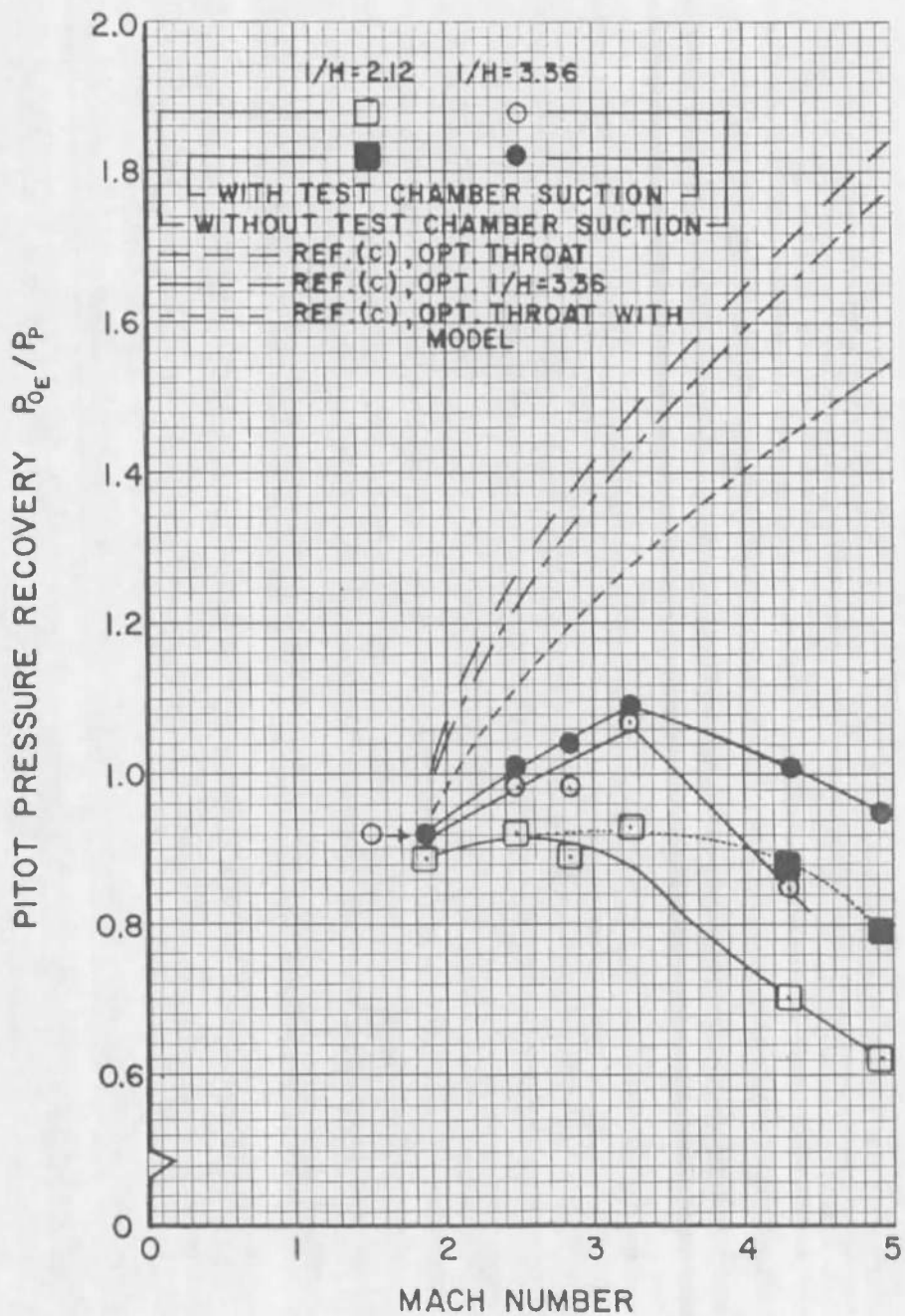


FIG.18 OPTIMUM PITOT PRESSURE RECOVERY

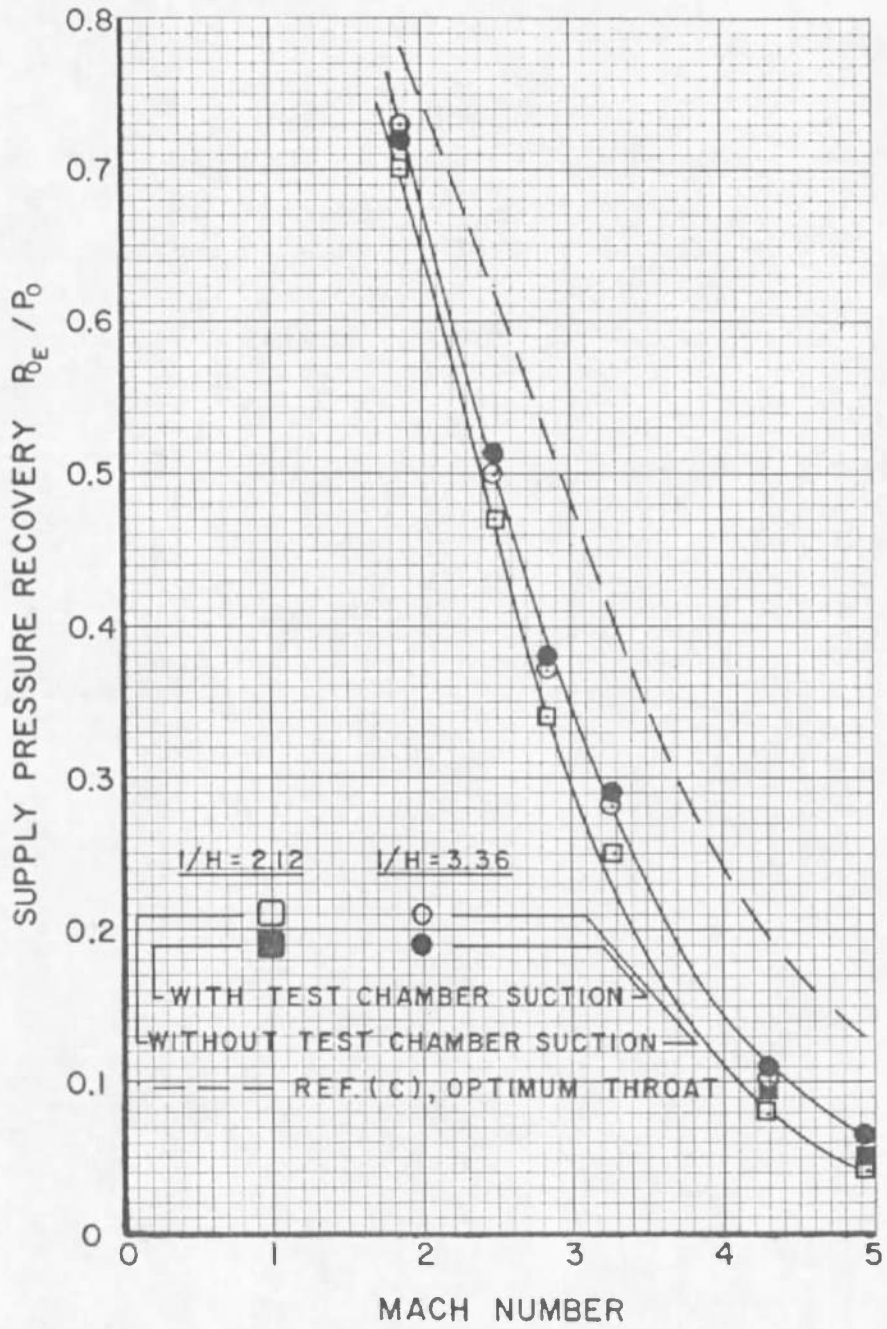


FIG. 19 OPTIMUM SUPPLY PRESSURE RECOVERY

M=1.86

l/H=2.12

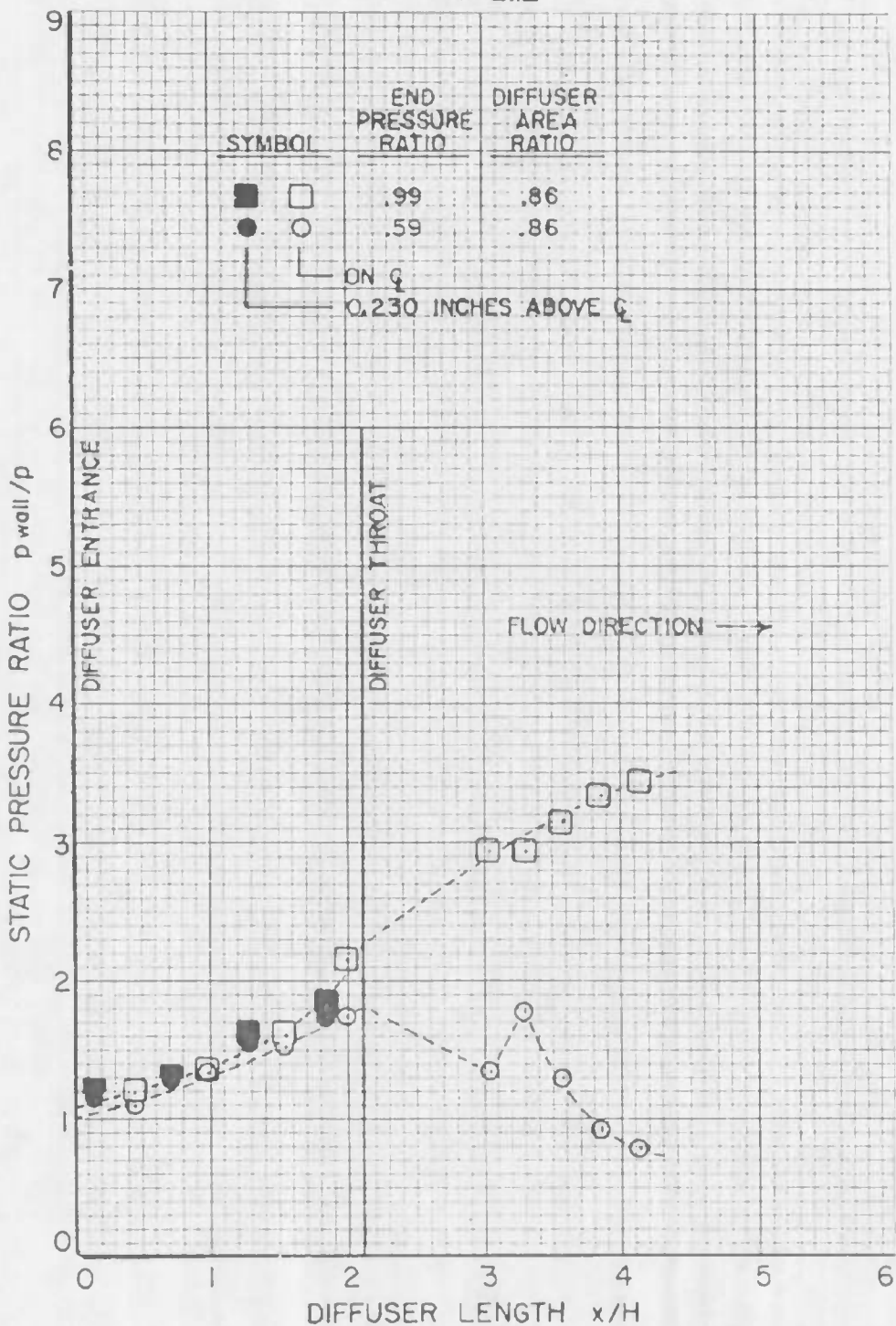


FIG.20 SIDEWALL STATIC PRESSURE DISTRIBUTION

$M = 1.86$

$l/H = 3.36$

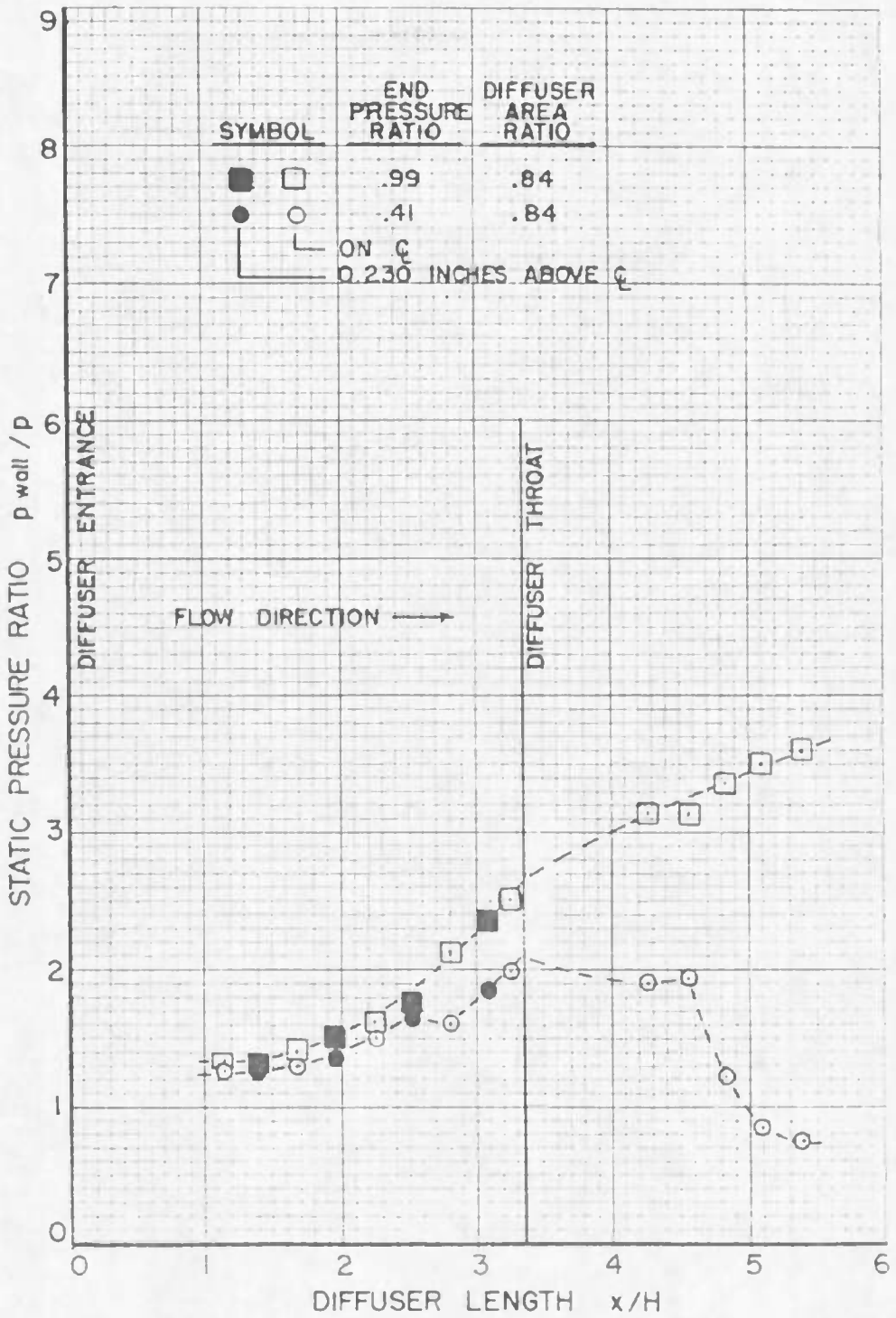


FIG. 21 SIDEWALL STATIC PRESSURE DISTRIBUTION

M=2.48

l/H=2.12

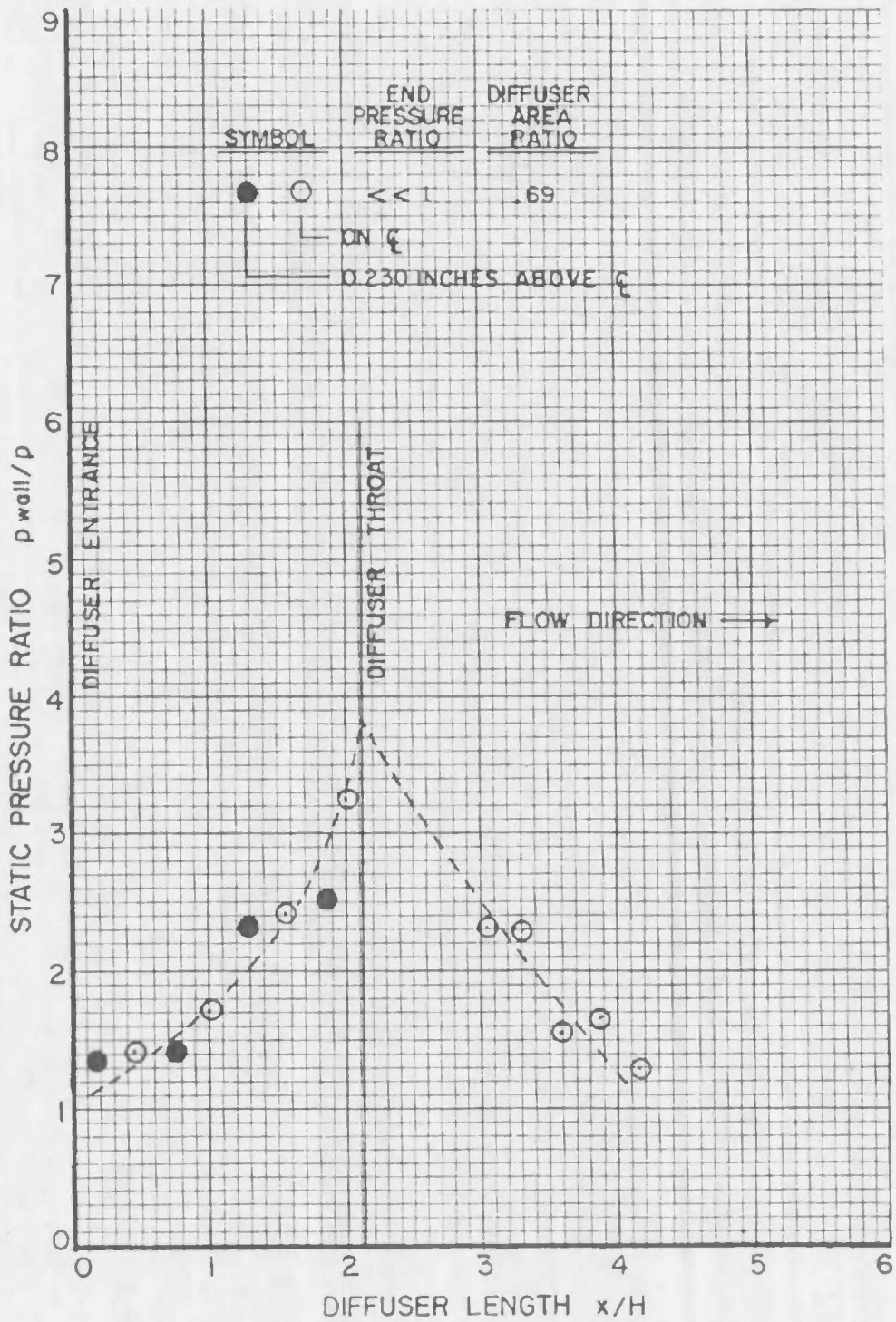


FIG.22 SIDEWALL STATIC PRESSURE DISTRIBUTION

$M = 2.48$

$l/H = 3.36$

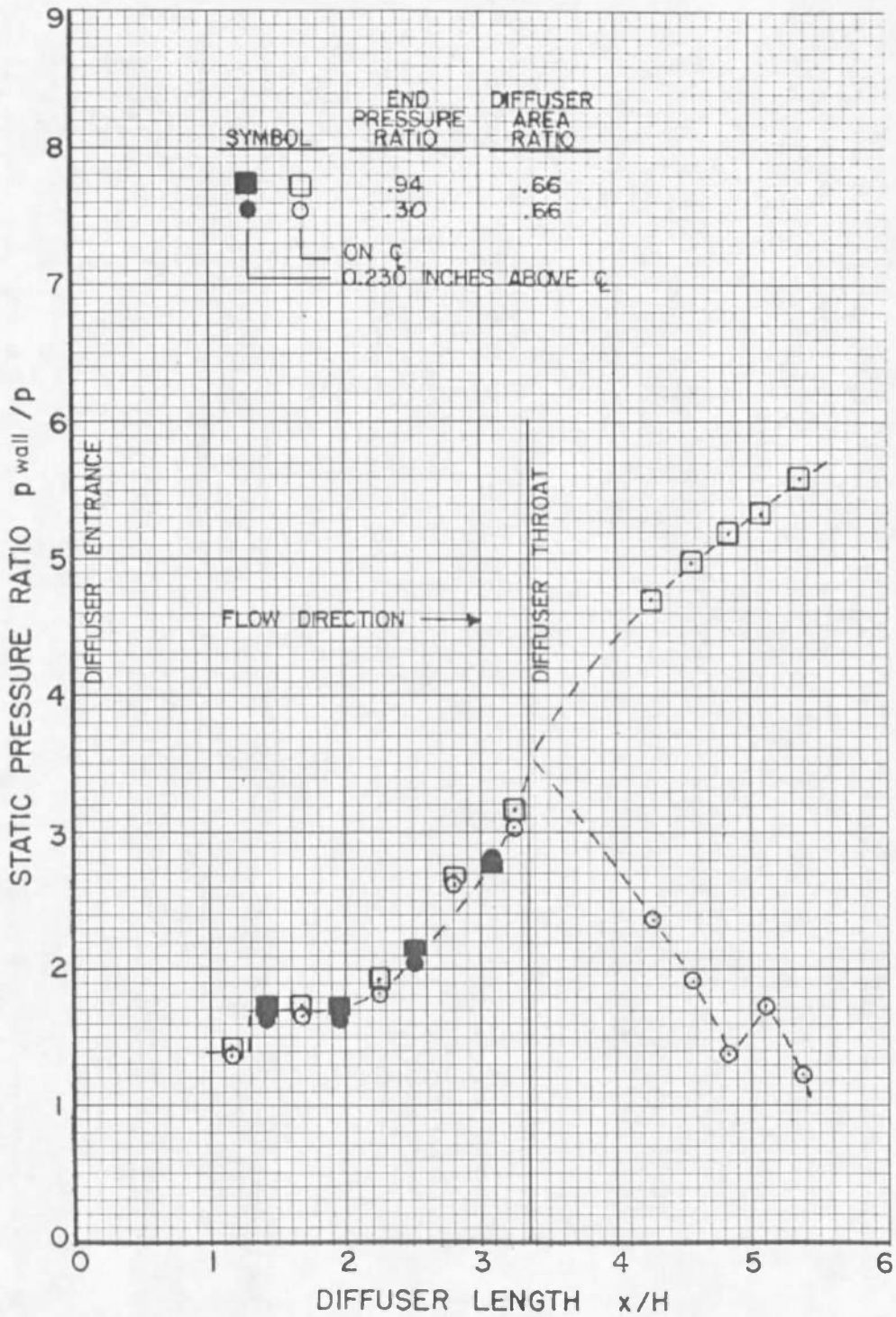


FIG. 23 SIDEWALL STATIC PRESSURE DISTRIBUTION

M=2.83

l/H= 2.12

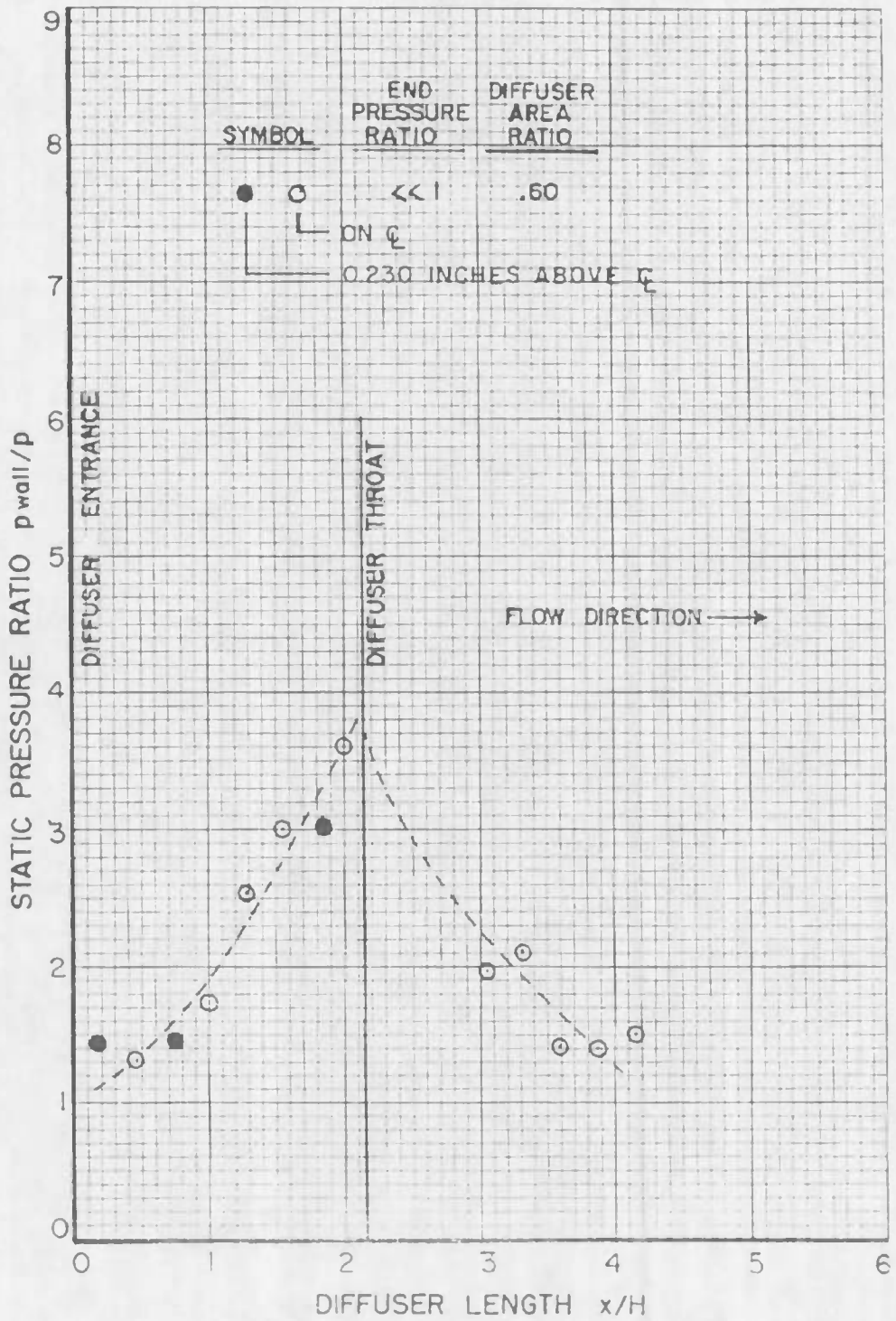


FIG. 24 SIDEWALL STATIC PRESSURE DISTRIBUTION

$M = 2.83$

$l/H = 3.36$

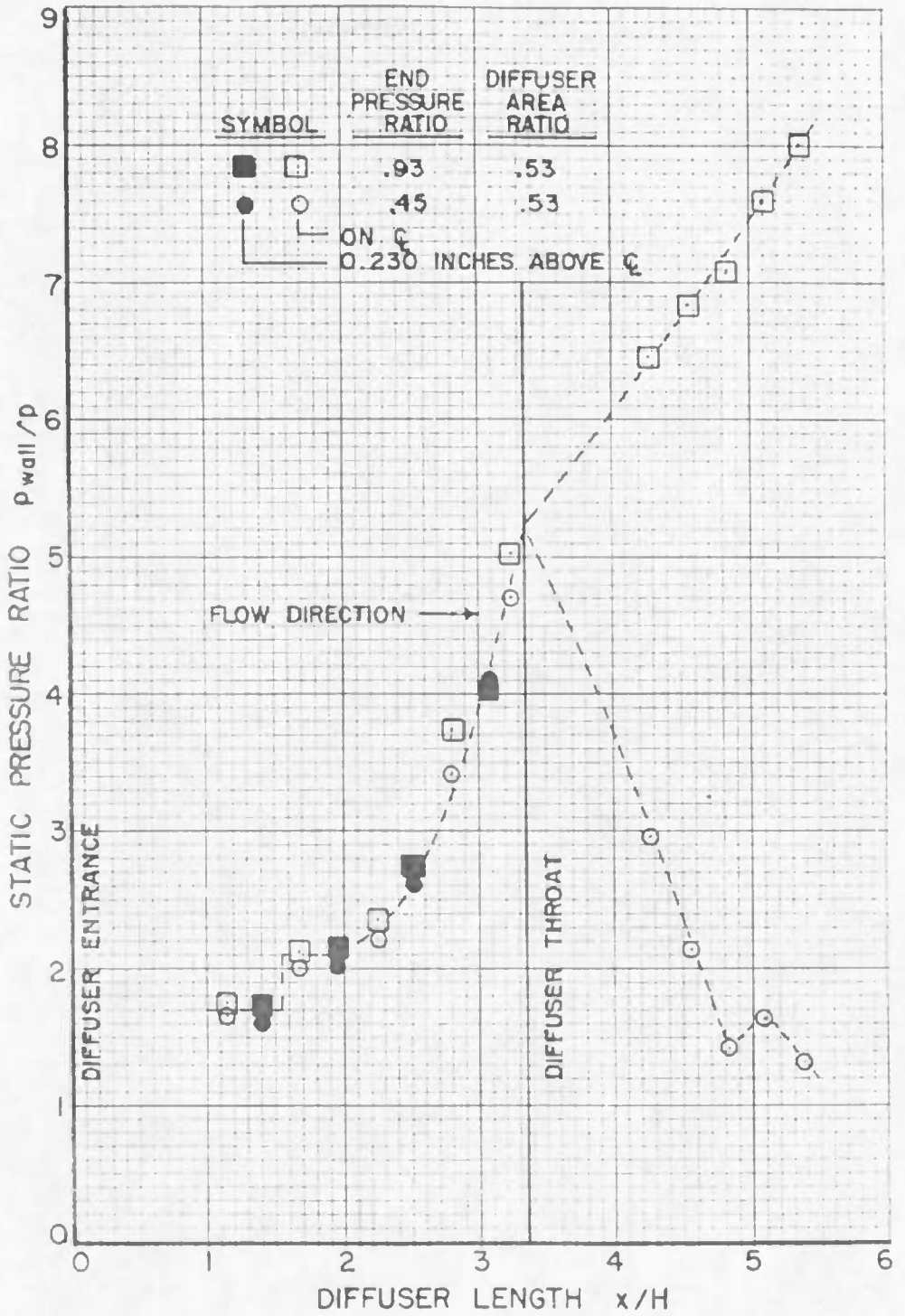


FIG. 25 SIDEWALL STATIC PRESSURE DISTRIBUTION

$M = 3.24$

$l/H = 2.12$

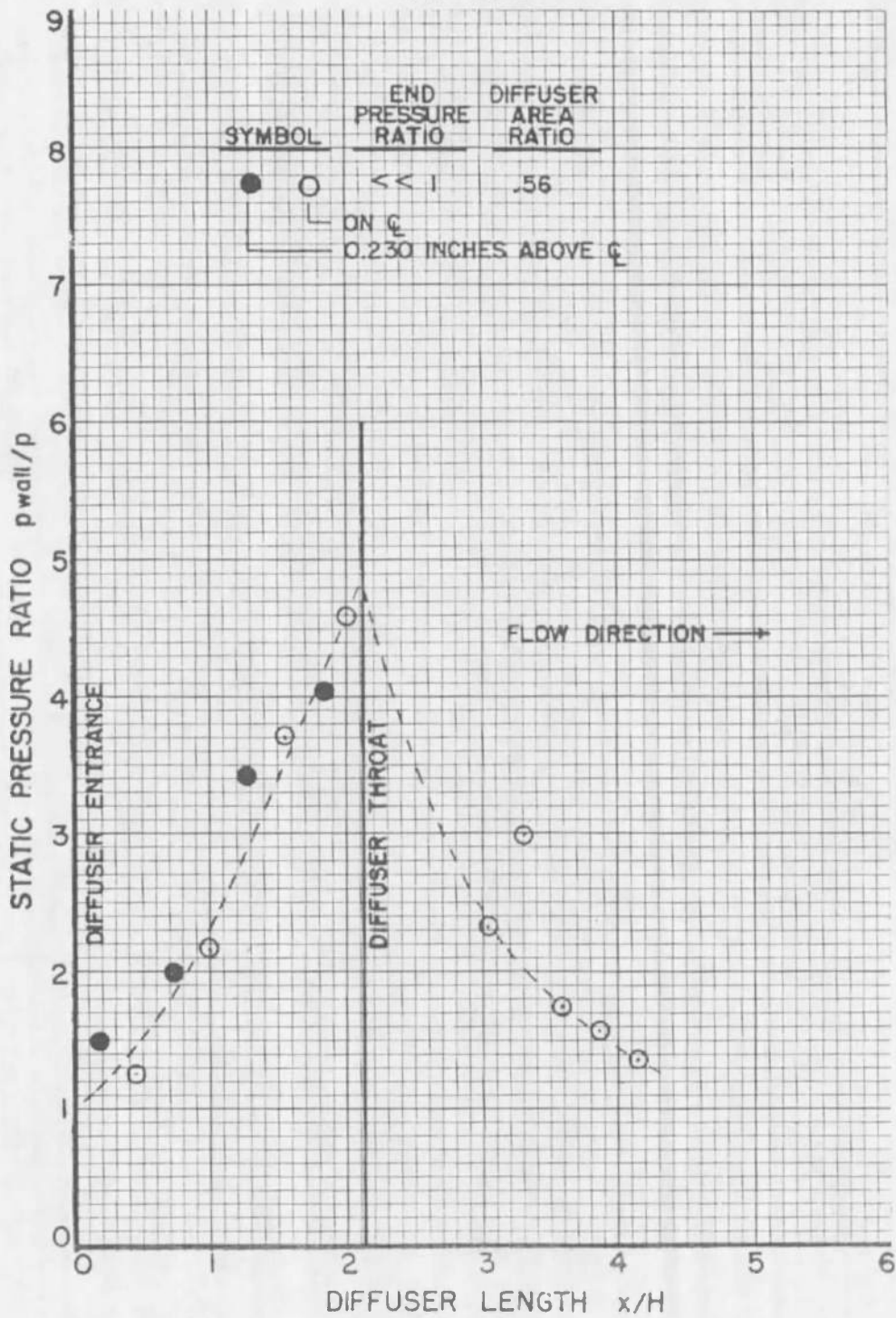


FIG.26 SIDEWALL STATIC PRESSURE DISTRIBUTION

$M = 3.24$

$l/H = 3.36$

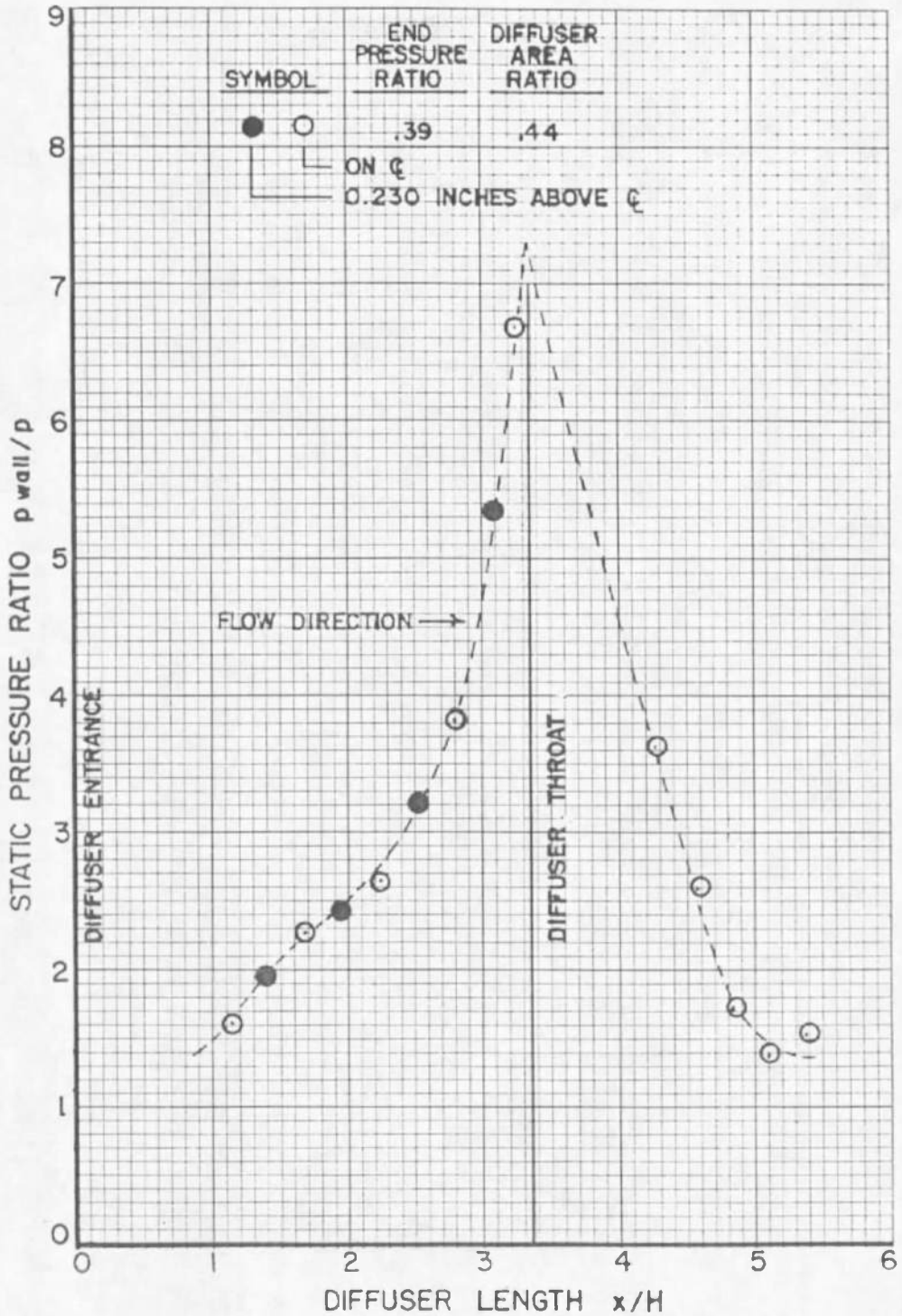


FIG.27 SIDEWALL STATIC PRESSURE DISTRIBUTION

$M = 4.30$

$1/H = 2.12$

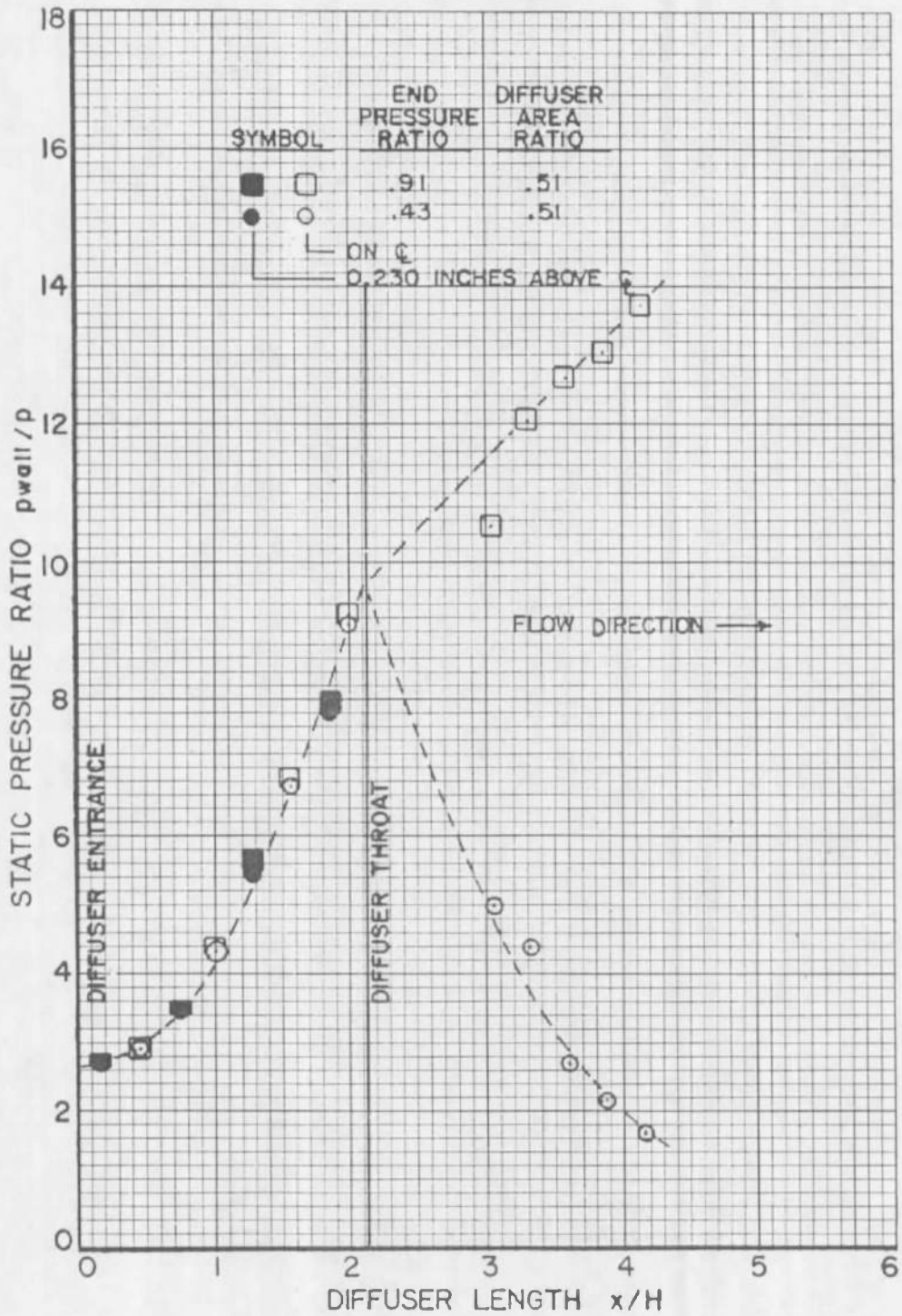


FIG.28 SIDEWALL STATIC PRESSURE DISTRIBUTION

$M = 4.30$

$l/H = 3.36$

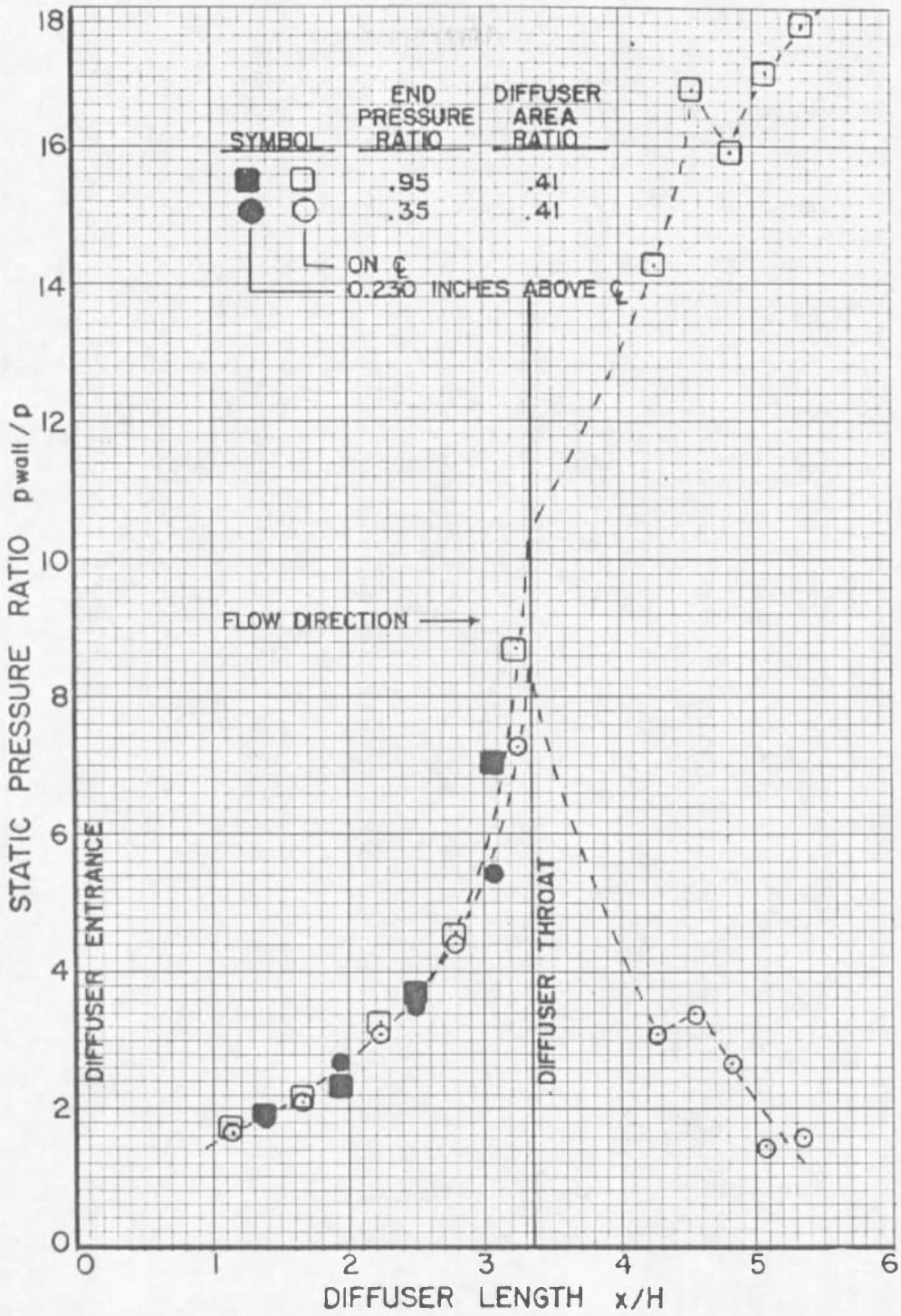


FIG.29 SIDEWALL STATIC PRESSURE DISTRIBUTION

M = 4.92

l/H = 2.12

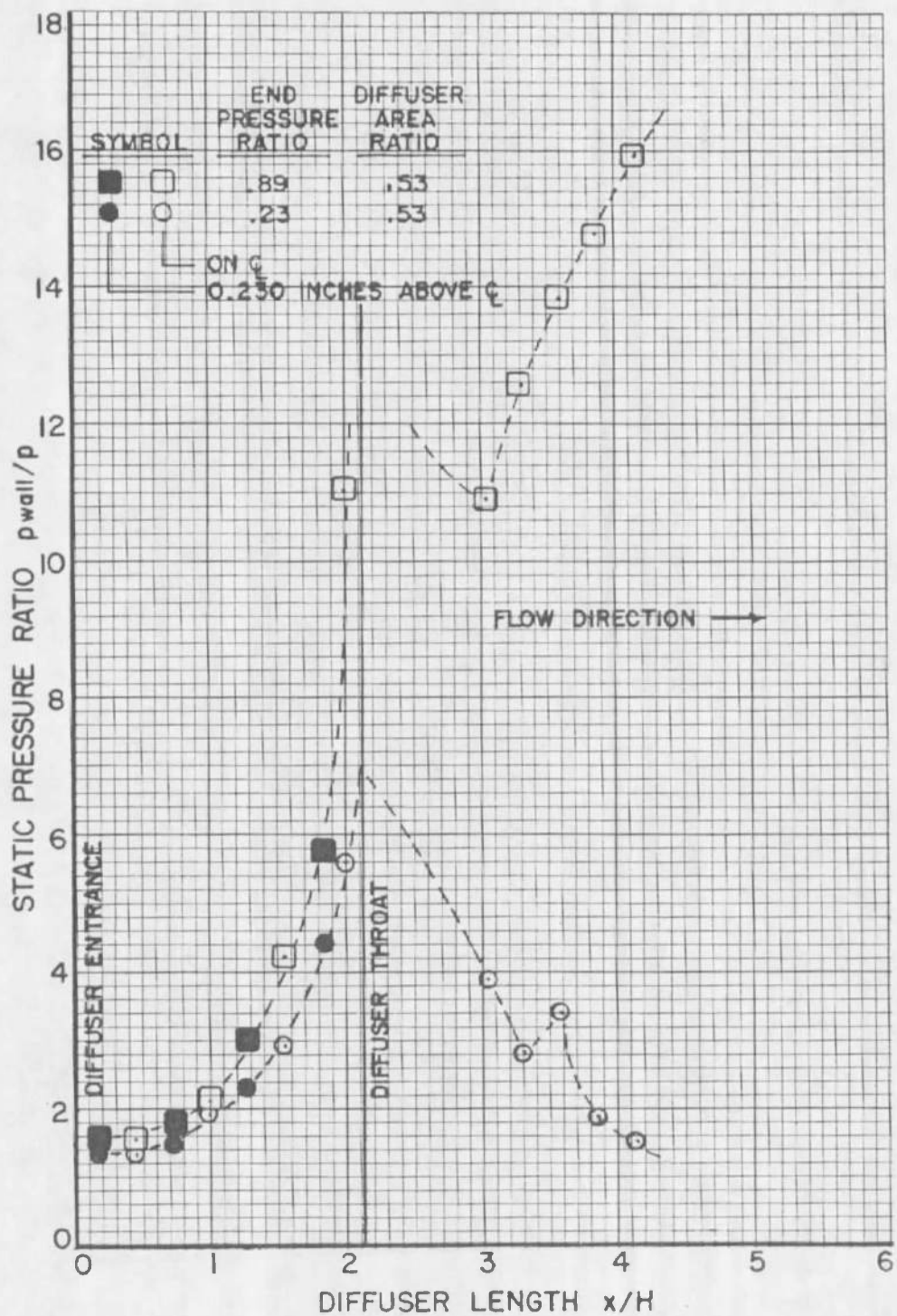


FIG.30 SIDEWALL STATIC PRESSURE DISTRIBUTION

$M = 4.92$

$l/H = 3.36$

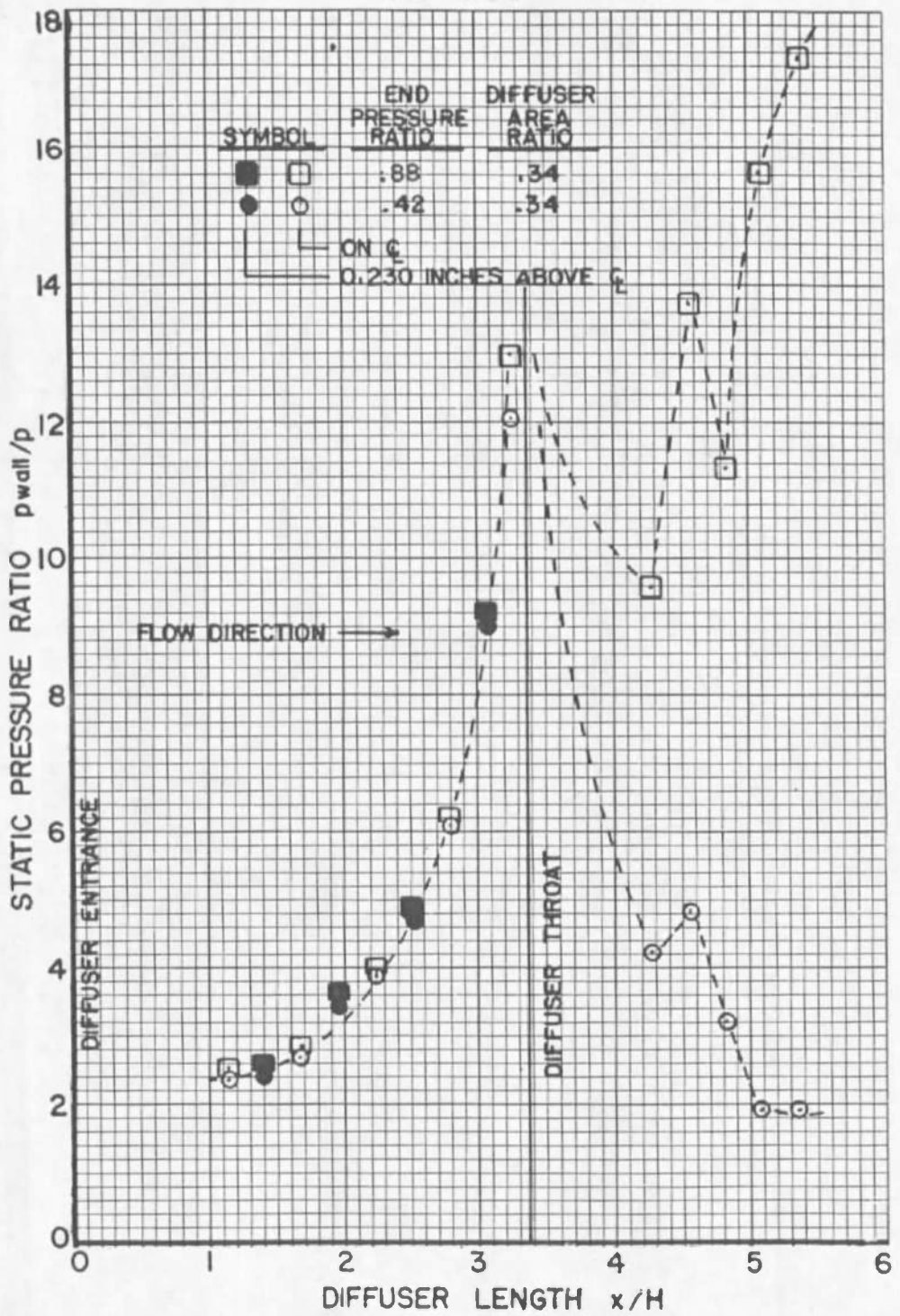
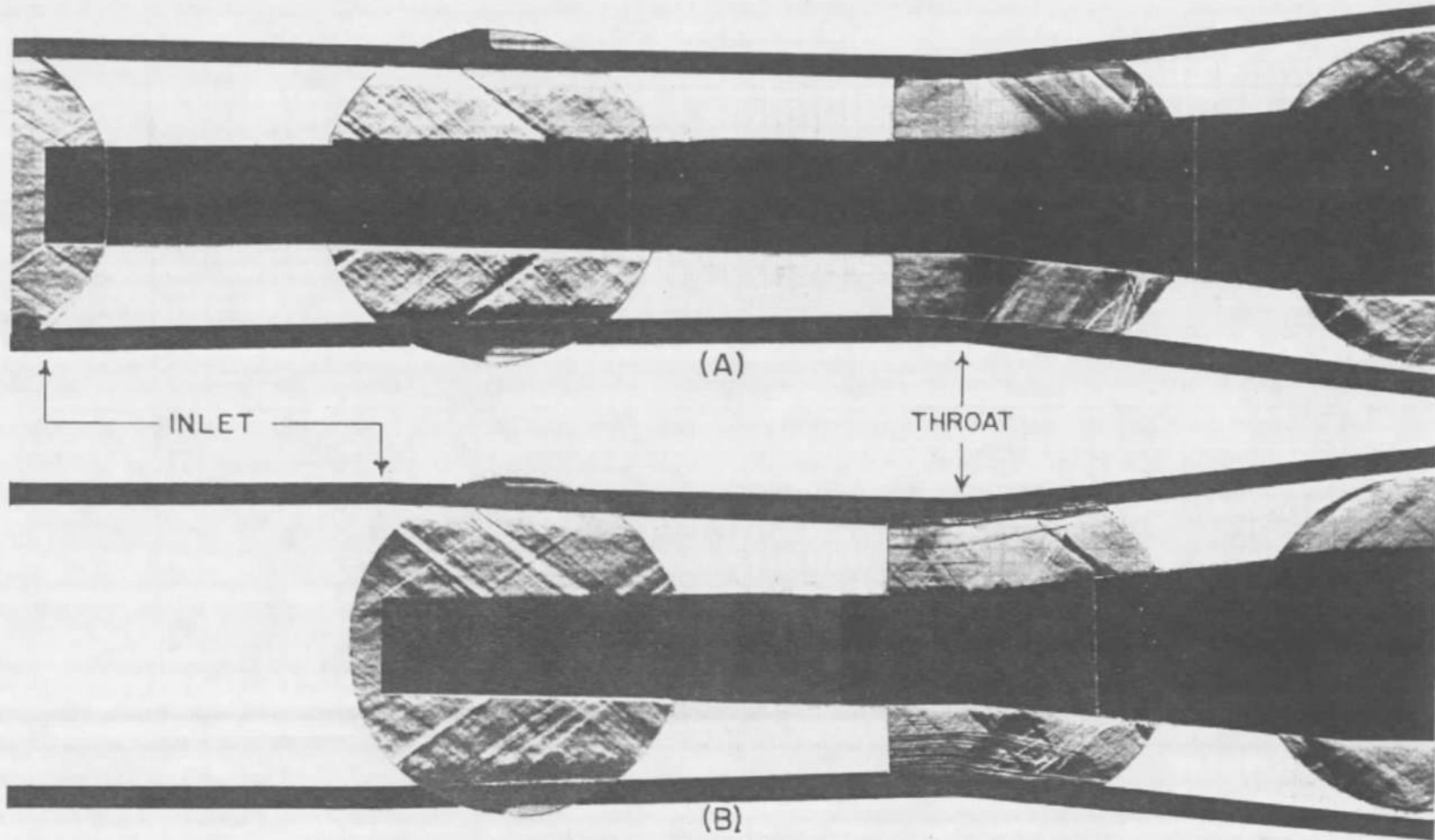
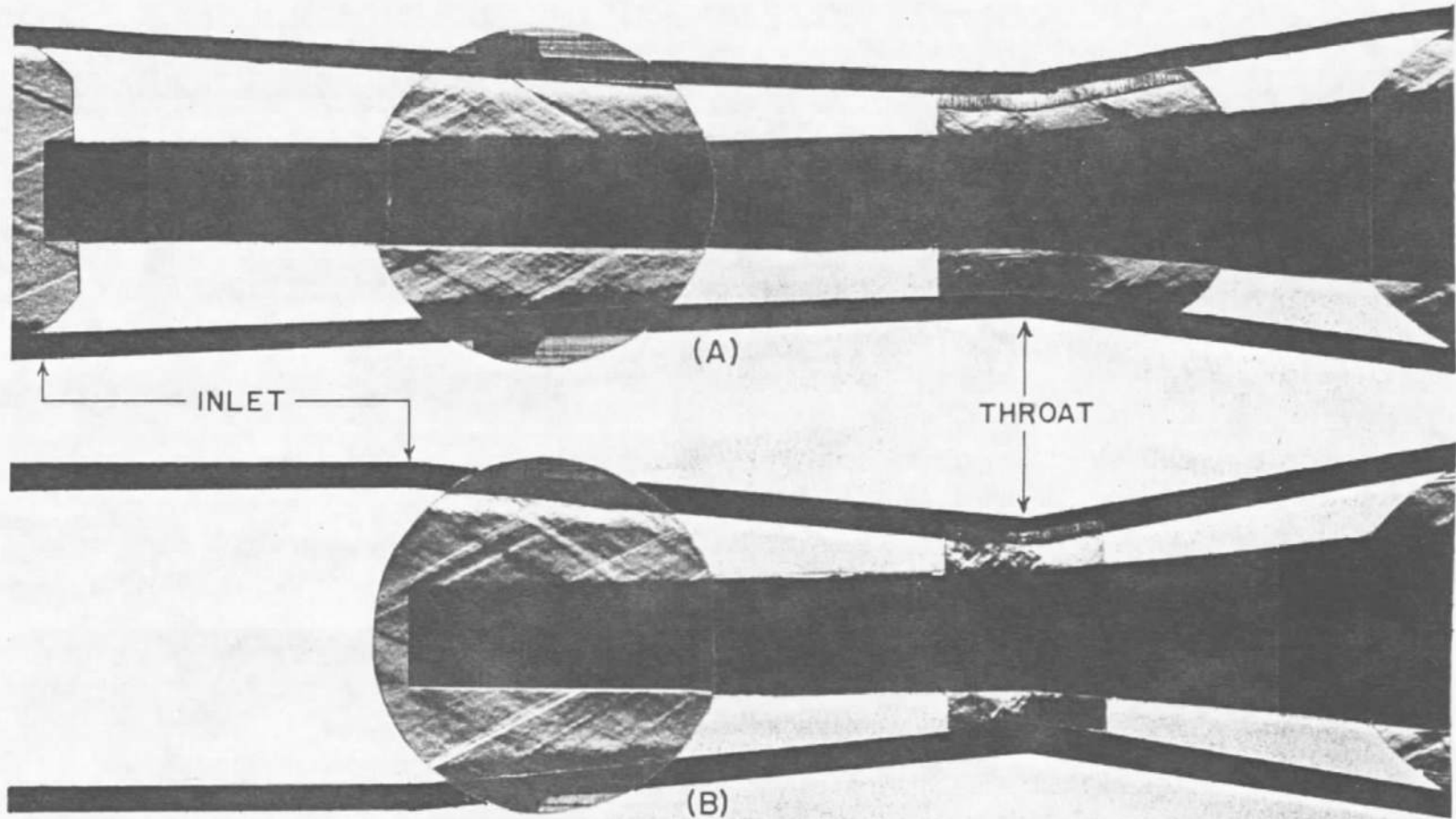


FIG.31 SIDEWALL STATIC PRESSURE DISTRIBUTION



- (A) $l/H=3.36$, DIFFUSER AREA RATIO = 0.84
- (B) $l/H=2.12$, DIFFUSER AREA RATIO = 0.88

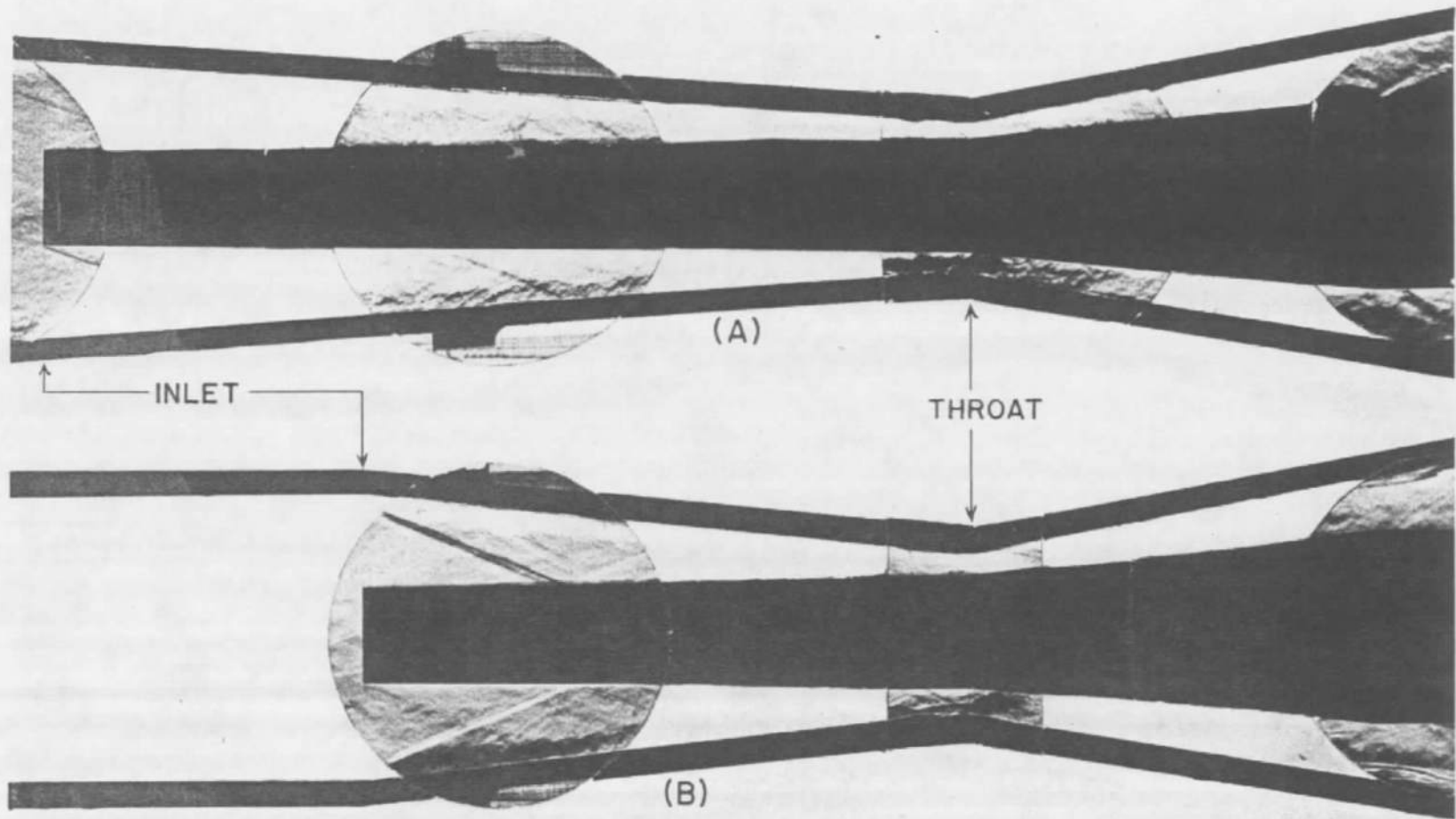
FIG.32 SCHLIEREN PHOTOGRAPHS OF THE FLOW AT $M=1.86$



(A) $1/H=3.36$, DIFFUSER AREA RATIO = 0.66

(B) $1/H=2.12$, DIFFUSER AREA RATIO = 0.70

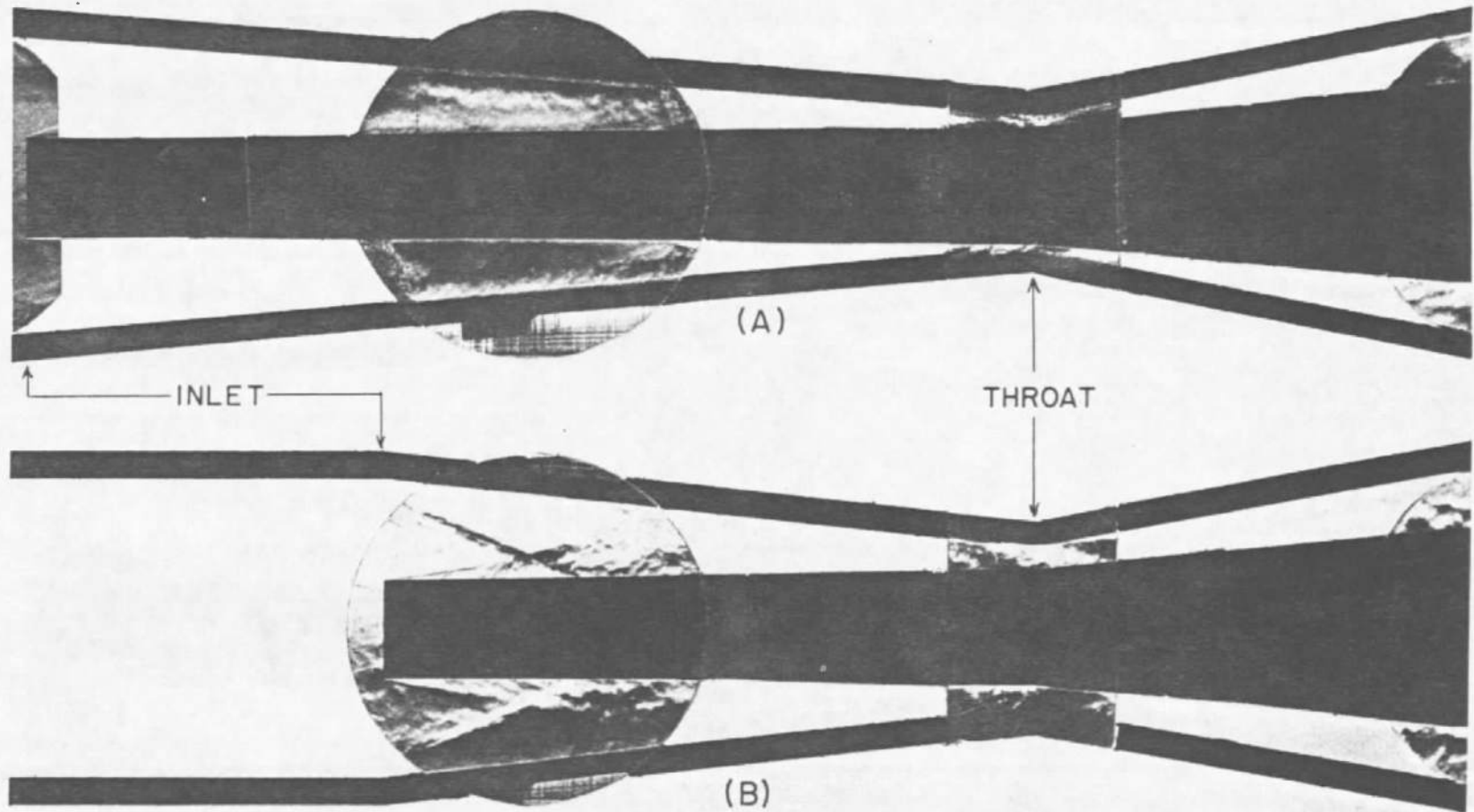
FIG.33 SCHLIEREN PHOTOGRAPHS OF THE FLOW AT $M=2.48$



(A) $1/H = 3.36$ DIFFUSER AREA RATIO = 0.46

(B) $1/H = 2.12$ DIFFUSER AREA RATIO = 0.56

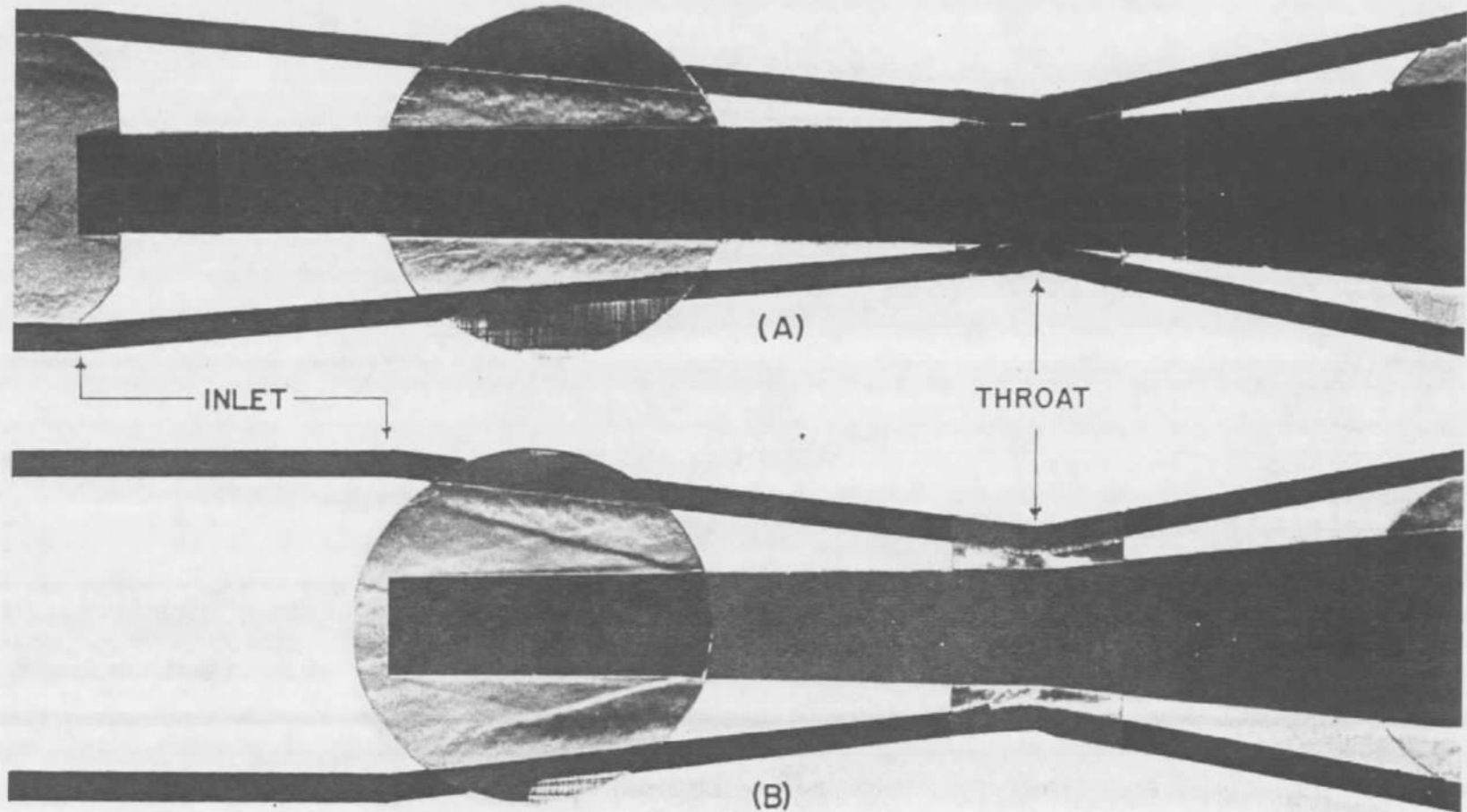
FIG.34 SCHLIEREN PHOTOGRAPHS OF THE FLOW AT $M = 3.24$



(A) $1/H = 3.36$, DIFFUSER AREA RATIO = 0.41

(B) $1/H = 2.12$ DIFFUSER AREA RATIO = 0.51

FIG.35 SCHLIEREN PHOTOGRAPHS OF THE FLOW AT $M = 4.30$



(A) $l/H=3.36$, DIFFUSER AREA RATIO = 0.32

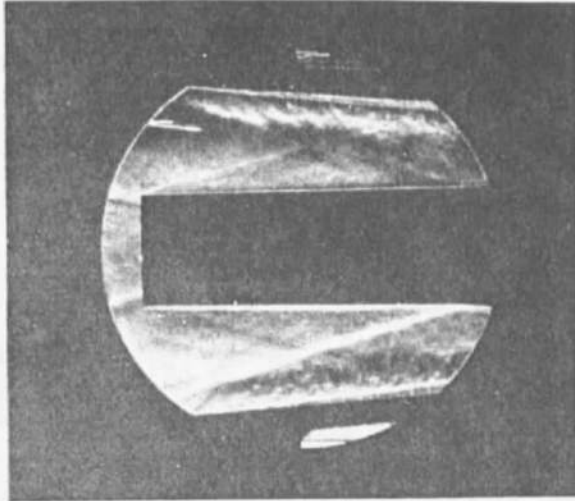
(B) $l/H=2.12$, DIFFUSER AREA RATIO = 0.53

FIG.36 SCHLIEREN PHOTOGRAPHS OF THE FLOW AT $M=4.92$

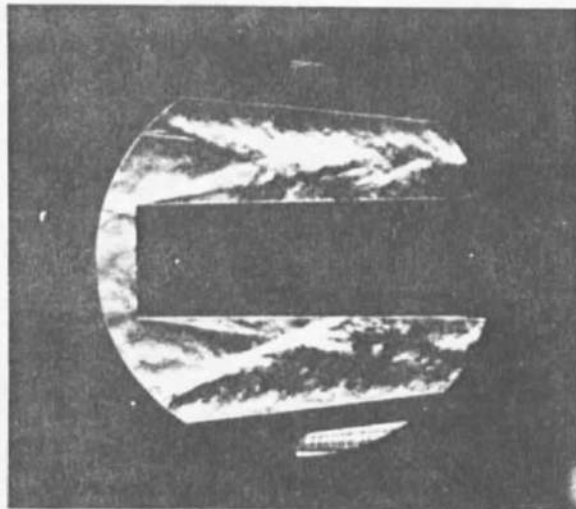
M = 4.30

END PRESSURE RATIO = 0.42

l/H = 2.12



DIFFUSER AREA RATIO = 0.66



DIFFUSER AREA RATIO = 0.51

FIG.37 EFFECT OF DIFFUSER AREA RATIO ON FLOW
IN THE SUPERSONIC DIFFUSER

AEROBALLISTIC RESEARCH DEPARTMENT EXTERNAL DISTRIBUTION LIST

No. of
Copies

1 Chief, Bureau of Ordnance
Department of the Navy
Washington 25, D. C.
Attn: Rexm

5 Commanding General
Arnold Engineering Development Center
Tullahoma, Tennessee
Attn: Major Claude J. Wilson, AEKS

2 ARO, Inc.
Arnold Engineering Development Center
Tullahoma, Tennessee
Attn: Mr. Heinrich Ramm

2 United Aircraft Corporation
400 Main Street
East Hartford 8, Connecticut
Attn: Mr. W. Kuhrt, Research Dept.

2 Defense Research Laboratory
University of Texas
P. O. Box 1, University Station
Austin, Texas
Attn: Dr. M. J. Thompson

2 University of Minnesota
Rosemount Research Laboratories
Rosemount, Minnesota
Attn: Mr. Richard De Leo

1 Dr. Rudolf Hermann

2 Sverdrup & Parcel, Inc.
Syndicate Trust Building
St. Louis 1, Missouri
Attn: Mr. M. Pindzola

1 Chief, Bureau of Aeronautics
Department of the Navy
Washington 25, D. C.
Attn: TD-4

1 Dr. O. E. Lancaster

1 Commander
U. S. Naval Ordnance Test Station
Inyokern, P. O. China Lake, California
Attn: Reports Unit

No. of
Copies

1 Commanding Officer
Naval Proving Ground
Dahlgren, Virginia
Attn: Dr. C. C. Bramble

1 Commander
U. S. Naval Air Missile Test Center
Point Mugu, California

1 Commanding Officer and Director
David W. Taylor Model Basin
Washington 7, D. C.
Attn: Hydromechanics Laboratory

Office of Naval Research
Department of the Navy :
Washington 25, D. C.
Attn: Mathematics Branch
1 Fluid Mechanics Branch
1 Mr. J. N. Heald
1 c/o Science and Technology Project
Library of Congress

Director
Naval Research Laboratory
Washington 25, D. C.
1 Attn: Code 2021
1 Superintendent, Mechanics Division

Commanding General
Aberdeen Proving Ground
Aberdeen, Maryland
1 Attn: Ballistic Research Laboratories
1 Mr. C. L. Poor, III

1 Department of the Army
Office, Chief of Ordnance
Pentagon
Washington 25, D. C.
Attn: ORDTU

1 Commanding General
Air University
Maxwell Air Force Base, Alabama
Attn: Air University Library

No. of
Copies

1 Headquarters, U. S. Air Force
Directorate of Research and Development
Washington 25, D. C.
Attn: AFDRD-AC2

1 Commanding General
Air Material Command
Wright-Patterson Air Force Base
Dayton, Ohio
1 Attn: Mr. D. Shore
1 TSEON-2
1 MCIDXD
1 Chief Scientist, OAR

1 Chairman
Research and Development Board
Pentagon
Washington 25, D. C.
Attn: Information Requirement Board
Room 3D1075

1 Director
National Advisory Committee for Aeronautics
1724 F Street, Northwest
Washington, D. C.
1 Attn: Dr. J. W. Crowley
1 Dr. I. H. Abbott
1 Office of Aeronautical Intelligence

1 Director
Ames Aeronautical Laboratory
Moffett Field, California
1 Attn: Mr. W. G. Vincenti
1 Mr. H. J. Allen

1 Director
Lewis Flight Propulsion Laboratory
Cleveland, Ohio
1 Attn: Mr. John C. Evvard
1 Mr. Abe Silverstein

1 Director
Langley Aeronautical Laboratory
Langley Field, Virginia
1 Attn: Mr. John Stack
1 Mr. Carl Kaplan

No. of
Copies

1	Massachusetts Institute of Technology Project METEOR Cambridge 39, Massachusetts Attn: Guided Missiles Library	VIA Development Contract Officer Massachusetts Institute of Technology Cambridge 38, Massachusetts
1	Professor J. D. Akerman Department of Aeronautical Engineering University of Minnesota Minneapolis, Minnesota	VIA Inspector of Naval Material Federal Building Milwaukee 2, Wisconsin
1	Consolidated-Vultee Aircraft Corp. Ordnance Aerophysics Laboratory Daingerfield, Texas Attn: Mr. J. E. Arnold	VIA Development Contract Officer Consolidated-Vultee Aircraft Corp. Daingerfield, Texas
1	Hughes Aircraft Company Florence Avenue at Teal Street Culver City, California Attn: Dr. A. E. Puckett	VIA Chief, Los Angeles APPFO 155 West Washington Blvd. Los Angeles 54, California
1	Mr. J. T. Milk	
1	Central Air Documents Office U. B. Building Dayton, Ohio	
1	Mr. Ronald Smelt Chief, Gas Dynamics Facility Arnold Research Organization Inc. Tullahoma, Tennessee	
1	Dr. F. H. Clauser Johns Hopkins University Department of Aeronautical Engineering Baltimore 18, Maryland	
1	Dr. G. N. Patterson Institute of Aerophysics University of Toronto Toronto 5, Canada	
1	Commanding General Redstone Arsenal Huntsville, Alabama Attn: J. L. Potter - ORDDW - MRF	